UNIVERSITY OF ECHAHID HAMMA LAKHDAR EL OUED
FACULTY OF TECHNOLOGY
Department of Mechanical Engineering

THESIS

ACADEMIC MASTER

Specialization: Electromechanical Engineering

Topic

Improving the performance of a photovoltaic system using optimization techniques (fuzzy logic)

Presented by:

- Souhail Mansouri
- Saad Yahia
- Nadim Mansouri

Defended on: 23/05/2026 Before the jury members:

- **Dr. Mosbah Laouamer**.. **President.**
- **Dr. Abdel Kader Mahmoudi**.. **Examiner.**
- **Dr. Soulef Larget** .... **Supervisor.**
- **Dr. Ali Babboukha**... **Co-supervisor.**

Academic Year 2025/2026

Dedication

I dedicate this modest work:

To my very dear parents

I find here the opportunity to express to them

my most sincere gratitude.

To my brother

To my sisters

To my supervisor

To all the teachers

To all my colleagues and friends

To all those who are dear to me.

Acknowledgements

My thanks go first of all to Almighty God, who has given me everything I possess and guided my steps toward the path of knowledge.

I would like to express my high gratitude, deep respect, and my most sincere thanks and appreciation, first to Mr. **Ali BABOUKHA**, who guided me with great patience throughout the development of this work.

I also extend my warm thanks to Mrs. **Soulaf LERKET**, for supervising us and for her valuable guidance.

Abstract

This study presents the development of a photovoltaic (PV) system using optimization techniques based on Fuzzy Logic Control (FLC) to improve system efficiency and energy extraction under varying environmental conditions. The proposed method enhances the Maximum Power Point Tracking (MPPT) process by providing fast response, reducing oscillations, and improving adaptability compared to conventional techniques. Simulation results demonstrate that the fuzzy logic approach significantly improves tracking accuracy, system stability, and overall PV performance, ensuring reliable and efficient operation under changing solar irradiance and temperature conditions.

Kaywords : photovoltaic (PV) system- Maximum Power Point Tracking- conventional techniques.

الملخص :

تُقدّم هذه الدراسة تطويرًا لنظام طاقة كهروضوئية (PV) باستخدام تقنيات التحسين القائمة على التحكم بالمنطق (FLC)، وذلك لتعزيز كفاءة النظام واستخلاص الطاقة تحت ظروف بيئية متغيرة. وتعمل الطريقة المقترحة على تحسين عملية تتبع نقطة الطاقة القصوى (MPPT) من خلال توفير استجابة سريعة، وتقليل التذبذبات، وتعزيز القدرة على التكيف مقارنة بالتقنيات التقليدية. كما تُظهر نتائج المحاكاة أن نهج المنطق الضبابي يحسّن بشكل كبير من دقة التتبع، واستقرار النظام، والأداء العام للمنظومة الكهروضوئية، مما يضمن تشغيلًا موثوقًا وفعالًا في ظل تغير ظروف الإشعاع الشمسي ودرجات الحرارة.

الكلمات المفتاحية : طاقة كهروضوئية- نقطة الطاقة القصوى- المنطق الضبابي.

Table of Contents

List of figures

List of tables

General Introduction

General Introduction

In light of the increasing global trend toward reducing carbon emissions and combating global warming, renewable energy has become an indispensable strategic necessity. Photovoltaic (PV) systems stand at the forefront of this transition due to their high reliability and low operating costs, making them a fundamental pillar in sustainable energy transition plans.

Despite this progress, the energy yield of solar panels remains a significant challenge; their performance is sharply affected by sudden atmospheric fluctuations, such as changes in solar irradiance and ambient temperature. Since the electrical characteristics of a solar cell are inherently non-linear, operating the system away from the "Maximum Power Point" (MPP) leads to a substantial loss of available energy.

To overcome these obstacles, it has become essential to integrate intelligent control algorithms characterized by flexibility and speed. Fuzzy Logic is considered one of the most powerful tools in this regard, owing to its superior ability to process imprecise data and make accurate control decisions in complex dynamic systems—without the need for an exact mathematical model—ensuring faster and more stable tracking of the maximum power point.

To demonstrate this approach, this study focuses on the applied aspect by constructing a precise simulation model and an integrated virtual environment using MATLAB/Simulink. This platform is utilized to design and test the proposed Fuzzy Logic Control (FLC) algorithm and compare its results with traditional methods under varying climatic conditions. The software allows for the analysis of system behavior in real-time and evaluates the improvement in energy efficiency and voltage stability, providing a comprehensive view of the proposed optimization's effectiveness prior to physical implementation.

In conclusion, this thesis aims to provide an advanced technical solution that contributes to enhancing the performance of photovoltaic systems and reinforces the role of Artificial Intelligence in managing renewable energy sources, supported by rigorous results extracted from an advanced simulation environment.

Chapter I

Solar Radiation and Photovoltaic Energy

I.1. Introduction :

Solar radiation is considered one of the most important renewable energy sources and the most abundant on Earth. It represents the primary source of energy for operating photovoltaic systems (PV). Photovoltaic energy, commonly referred to as solar energy, is defined as the energy obtained through photovoltaic cells capable of converting sunlight directly into electrical energy by means of the photovoltaic effect.

This chapter provides a general overview of the concepts of solar energy. It addresses the fundamental principles upon which photovoltaic systems are based, in addition to explaining the mechanism of electricity generation through the photovoltaic effect. Furthermore, it highlights how the availability of solar energy varies according to geographical location and seasonal changes, which directly affects the efficiency and performance of these systems.

I.2. Solar Radiation :

Solar radiation is defined as the totality of radiations emitted by the Sun in its various forms. In addition to cosmic rays, which consist of particles characterized by extremely high speeds and energies, the Sun emits a broad spectrum of electromagnetic waves extending from radio waves to gamma rays, passing through the visible light range.

The emission of electromagnetic radiation from the Sun can be accurately described using the blackbody model at a temperature of approximately 5800 Kelvin, in accordance with Planck’s law. The peak of the emission occurs in the yellow region of the visible spectrum at a wavelength of approximately 570 nanometers ($\lambda \approx 570$ nm). Moreover, solar radiation is distributed almost evenly between the visible and infrared ranges, while ultraviolet radiation represents only a small fraction, not exceeding about 1% of the total radiation.

Upon reaching sea level, after passing through the Earth's atmosphere, solar radiation undergoes several filtering and absorption processes that affect its spectral characteristics. Among the most significant of these processes is the absorption of a large portion of ultraviolet radiation by ozone, in addition to absorption effects caused by oxygen, carbon dioxide, and water vapor, leading to the appearance of distinctive absorption bands in the solar spectrum at the Earth's surface[1] .

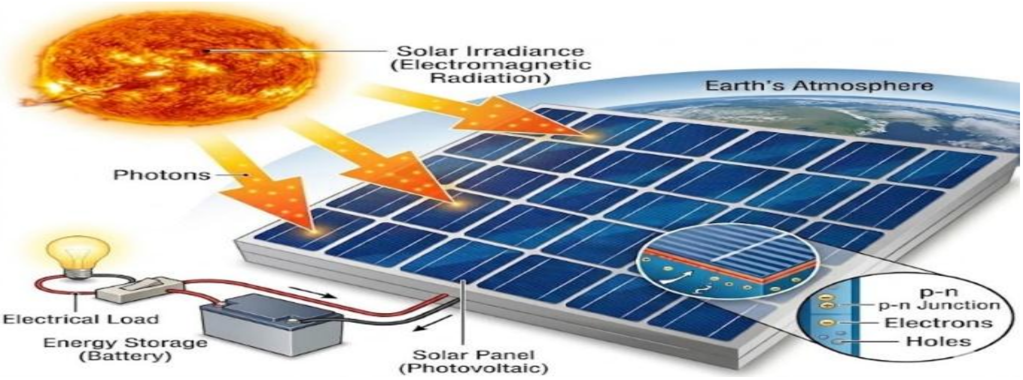

Figure I.1. Representation of Solar Radiation

I.2.1. Radiation Spectrum:

The concept of solar energy may appear abstract; however, in reality, it is represented by the light and heat we naturally receive from the Sun. The invention of photovoltaic cells in the last century has enabled the utilization of this energy source to power human civilization. Photovoltaic solar panels directly convert light energy into usable electric current.

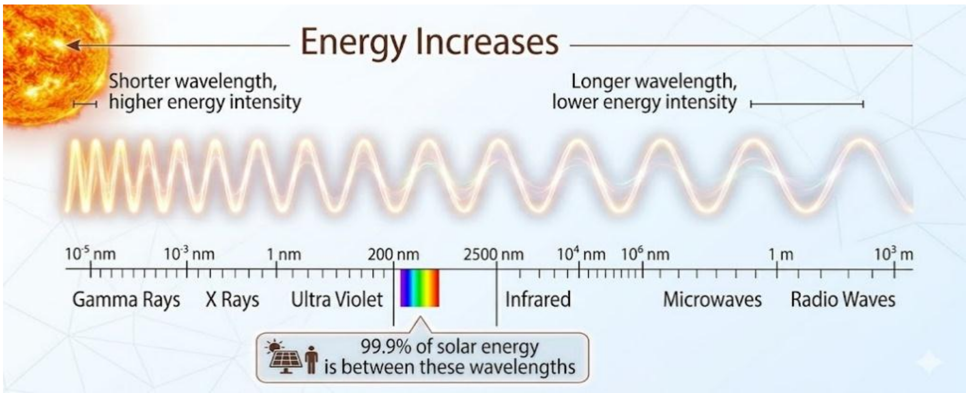

Figure I.2. Solar Radiation Spectrum

Although the electromagnetic spectrum is very wide, approximately 99.8% of solar radiation is emitted within a relatively narrow spectral range between 20 and 2500 nanometers. Only a limited portion of this radiation reaches the Earth’s surface, including some long-wavelength radio waves that may extend to several decameters, as well as weak ultraviolet radiation. In contrast, the majority of solar radiation is either absorbed or reflected as it passes through the atmosphere and the ionosphere [2].

Figure (1.3) illustrates the solar radiation spectrum. The composition of solar energy is approximately 5% ultraviolet light; 42% visible light and 53% near infra-red radiation.

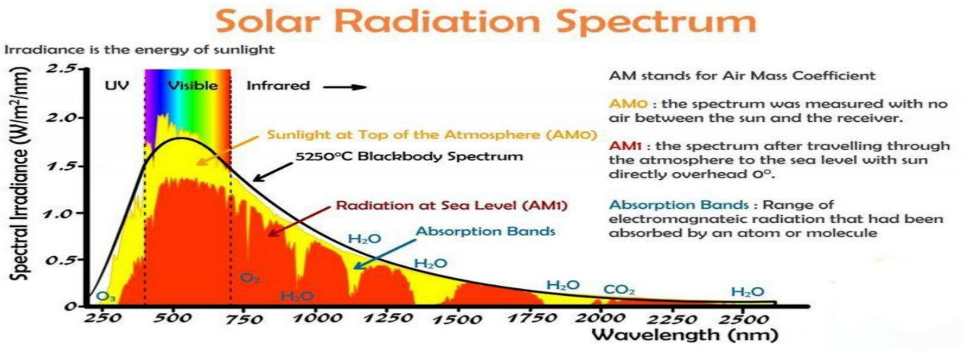

Figure I.3. Representation of Solar Radiation Spectrum

I.3. Conversion of Solar Radiation by PV Effect:

A photovoltaic (PV) cell consists of two layers of silicon that are doped with specific impurities to impart different electrical properties. One layer is doped with boron atoms to form a positive layer (P-type), while the other is doped with phosphorus atoms to create a negative layer (N-type), resulting in the formation of a potential barrier between them.

When this semiconductor is exposed to light radiation with sufficient energy, the absorbed photons break the covalent bonds within the crystal lattice, releasing electrons and generating positive holes. This phenomenon is known as the photovoltaic effect, where a potential difference is established between the two layers due to charge separation. When the two layers are connected through an external circuit, electrons flow from one layer to the other, thereby generating a direct electric current [1].

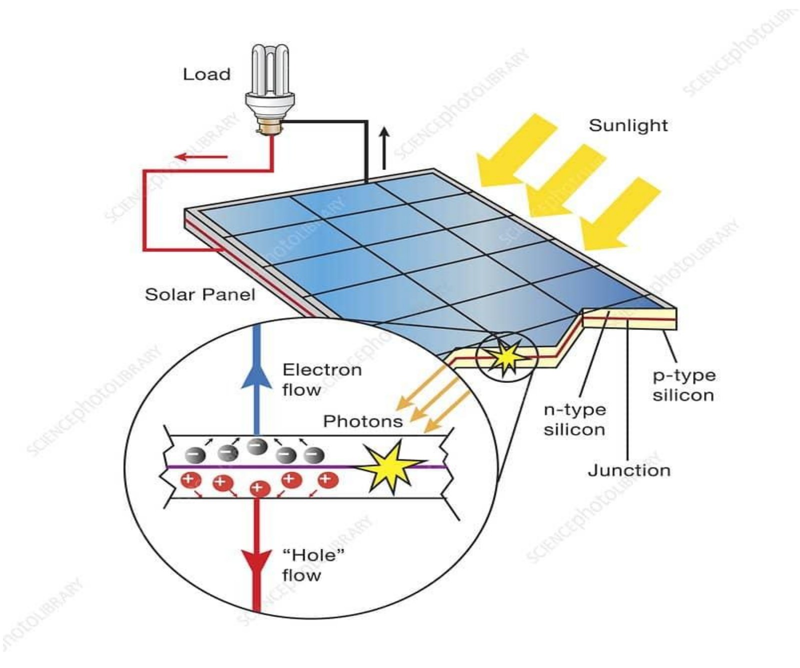

Figure I.4. Solar Radiation Conversion by PV Effect

I.4. Photovoltaic Generator:

The photovoltaic sensor is characterized by its electrical properties, particularly the relationship between current and voltage (I = f (V)), as illustrated in Figure (1.5).

This modelling is commonly used to estimate the sensor output (voltage, current) based on two input variables: temperature and the illumination received by the sensor.

The photovoltaic sensor is characterized by its electrical properties, which are primarily expressed through the current–voltage relationship (I = f(V)) , as illustrated in Figure (1.5). This model is widely used to estimate the sensor output, namely voltage and current, based on two main variables: temperature and the solar irradiance incident on the cell.

The current generated by the photovoltaic module at a given voltage depends directly on both the level of illumination and the cell temperature. When these two factors are kept constant, the efficiency of the solar cell is influenced by the nature of the electrical load connected to the circuit.

In the cases of open-circuit condition (Rc = ∞ , I = 0 , V = V_{oc}) and short-circuit condition (Rc = 0, I = I_{sc} , V= 0) , no power is delivered to the external load. Between these two extremes, there exists an optimal value of the load resistance (R_{opt}) , at which the solar cell delivers its maximum power to the load. This maximum power is defined by the relation:

($P=V_{max} \times I_{max}$) provided by the solar cell to the load resistance is maximal, thus reaching P_{max} [2].

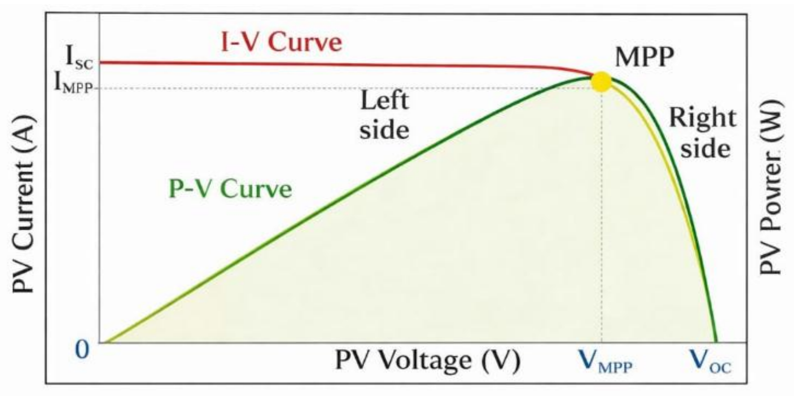

Figure I.5. Typical Characteristics of a PV Generator

The efficiency of a solar cell is defined by the following relation:

$\eta = P/P_{\gamma}$, where P_{γ} represents the incident light power on the surface of the cell, and P denotes the electrical power generated by the cell.

When the optimal load resistance R_{opt} is selected, the efficiency reaches its maximum value, expressed as:

$$\eta_{max} = \frac{P_{max}}{P_{\gamma}} \quad \textbf{(I.1)}$$

Studies show that the efficiency of solar cells decreases with increasing temperature. This has led to the development of hybrid systems combining photovoltaic cells with thermal collectors. These systems enable the utilization of the generated heat for water heating while simultaneously improving photovoltaic performance through cell cooling.

The electrical power generated by the solar cell is given by:

$$P = I \times V \quad \textbf{(I.2)}$$

This power, as well as the cell efficiency, depends on several technical and physical factors. These include the type of semiconductor material used (such as amorphous silicon, polycrystalline silicon, and monocrystalline silicon), the manufacturing technology, and the geometrical structure of the cell (e.g., layer thickness and multilayer configurations). It is also influenced by external operating conditions such as temperature, the spectrum and intensity of the incident radiation, and the characteristics of the external electrical circuit connected to the cell.

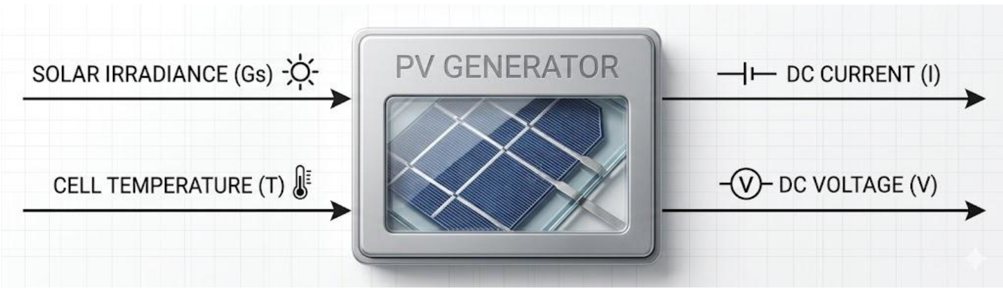

Figure I.6. Block Diagram of a PV Generator

I.4.1. Photovoltaic Cell:

Photovoltaic modules are composed of a set of electrically interconnected solar cells. These cells are encapsulated within a protective resin material and covered by external protective layers, either in the form of two tempered glass sheets in so-called (double-glass modules) , or a front glass layer combined with a Tedlar backsheet in (glass/Tedlar modules) . Typically, these modules are mounted within anodized aluminum frames to ensure mechanical strength and environmental protection. However, frameless modules are also employed in building-integrated photovoltaic (BIPV) applications, particularly on façades and rooftops.

The nominal power of a photovoltaic module depends on both its surface area and the incident solar irradiance. It is expressed in peak watts (Wp), which represents the maximum power the module can deliver under standard test conditions, corresponding to a solar irradiance of (1000 w/m^2).

The output voltage of a module is determined by the number of cells connected in series. For low-power modules (less than 75 Wp), the operating voltage typically ranges between 12 and 15 volts. In higher power modules, the voltage is increased by adding more cells in series, while the current is enhanced by increasing the number of parallel-connected branches. Consequently, the operating voltage may reach 24 volts or higher, depending on the requirements of the electrical system being supplied.

The surface area of photovoltaic modules varies among manufacturers, generally ranging from 0.5 to 1 square meter, and may extend up to 3 square meters in special applications or large-scale production. Interconnecting multiple modules results in a photovoltaic panel, while combining several panels forms a complete photovoltaic array. Furthermore, series and/or parallel configurations of modules enable the generation of different levels of voltage, current, and power, in accordance with the requirements of the intended application. [1].

I.4.2. Modelling of a PV Cell:

The behavior of a photovoltaic module is described using the standard one-diode model, originally developed by Shockley to represent a single photovoltaic cell, and later generalized to photovoltaic modules by considering them as assemblies of identical cells connected in series and/or in parallel.

In the scientific literature, a photovoltaic cell is typically modeled as an electrical current source, whose equivalent behavior consists of a current source connected in parallel with a diode. To achieve a more accurate representation of the physical phenomena occurring within the cell, this model is enhanced by incorporating two additional resistances: the series resistance R_s and the shunt resistance R_{sh} , as illustrated in the equivalent circuit.

The series resistance R_s accounts for the various contributions associated with the internal resistance of the cell, including the resistance of the semiconductor material, the contact resistance at the electrodes, and the resistivity of the collecting grids. In contrast, the shunt resistance R_{sh} represents the effect of leakage currents across the junction and is mainly related to the manufacturing quality and structural properties of the junction.

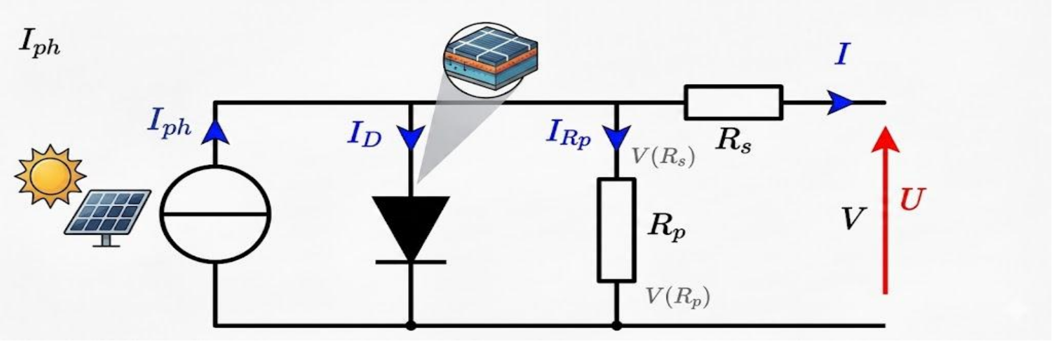

Figure I.7. Equivalent Circuit of a PV Cell

I.4.3. Types of Photovoltaic Cells :

Photovoltaic solar panels are composed of a set of photovoltaic cells, which differ in their physical and technical characteristics depending on the type of material used and the manufacturing technologies employed. These cells can be classified into several main types as follows:

I.4.3.1. Monocrystalline Cells:

This type is manufactured from monocrystalline silicon obtained through a controlled cooling process of molten silicon, resulting in a uniform crystal structure. The solidified crystal is then sliced into thin wafers used in the fabrication of photovoltaic cells. These cells are characterized by a homogeneous dark blue color and the absence of visible crystal defects, reflecting the high purity of their structure.

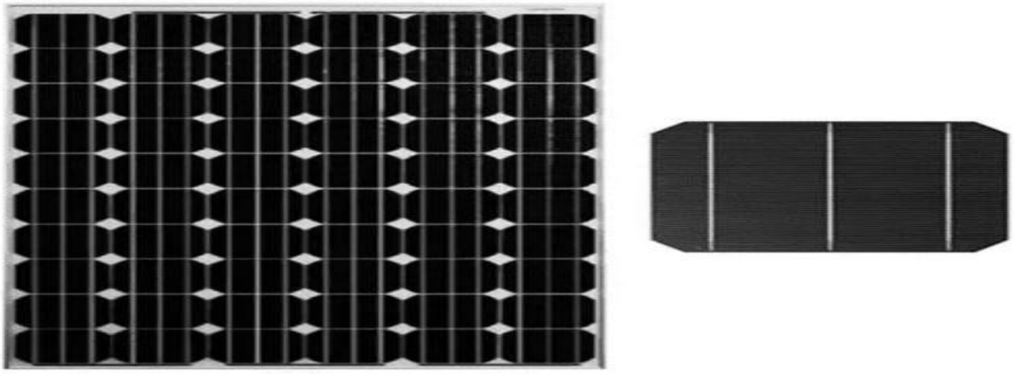

Figure I.8. Monocrystalline Cells

I.4.3.2. Polycrystalline Cells:

This type is produced by melting silicon and casting it into metal molds in the form of ingots. The material then cools in a non-uniform manner, leading to the formation of multiple crystals within the structure. These ingots are subsequently sliced into thin wafers to form photovoltaic cells. The resulting cells exhibit a bluish color with visible crystalline patterns caused by the different orientations of the crystals, which is a distinctive feature of this type.

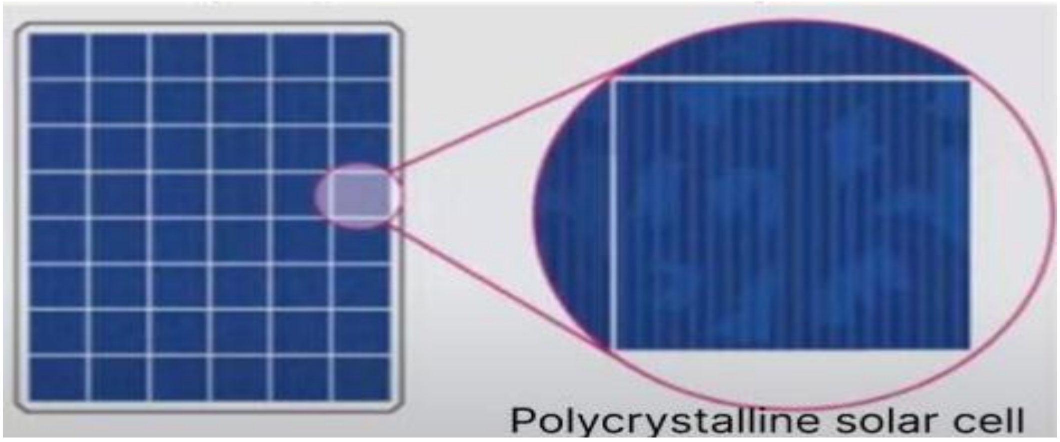

Figure I.9. Polycrystalline Cells

I.4.3.3. Hydrogenated Amorphous Cells:

This type is produced from silicon in its amorphous state, derived from silicon gas, which is deposited onto various substrates such as glass, flexible plastic, or metal using vacuum deposition techniques. These cells are characterized by a dark gray color and a non-uniform structure, which affects their electrical properties compared to crystalline cells.

Figure I.10. Hydrogenated Amorphous Cells

I.5. The Impact of Temperature on Solar Panel:

Temperature has a significant impact on the performance of solar panels, as follows:

- **Reduction in Efficiency:** As the temperature of solar panels increases, their efficiency decreases. Solar panels rely on converting solar radiation into electrical energy, and an increase in temperature leads to a decline in the efficiency of this conversion process.
- **Voltage Decrease:** The voltage of a solar panel decreases as temperature increases. This is due to the reduced efficiency of the semiconductor material in transporting electrical charges at higher temperatures.
- **Power Output Reduction:** An increase in temperature leads to a reduction in the electrical power output of solar panels, as a result of the negative effect of the decrease in both voltage and efficiency on the total power output.
- **Thermal Degradation:** High temperatures can lead to gradual thermal degradation of solar panel materials over time, which negatively affects their lifespan and operational efficiency.
- **Operating Temperature Range:** Solar panels are designed to operate within a specific temperature range, and if this range is exceeded, their performance deteriorates further.

Overall, although solar panels continue to generate electricity in hot conditions, higher temperatures lead to a decrease in their efficiency, which affects overall performance and productivity.

I.6. Advantages and Disadvantages of PV Energy:

I.6.1. Advantages:

- **Renewable Energy**: Solar energy is considered a renewable, abundant, and widely available global resource, making it a sustainable option for meeting long-term energy needs.
- **Low Greenhouse Gas Emissions**: Solar energy produces no greenhouse gas emissions during operation, which helps reduce carbon emissions and mitigate the effects of climate change.
- **Decreasing Costs**: Solar energy technologies have experienced a significant reduction in costs in recent years, which has enhanced their competitiveness compared to traditional energy sources.

- **Energy Independence**: Photovoltaic systems enable self-generation of electrical energy, reducing reliance on power supply grids and limiting the impact of energy price fluctuations.
- **Low Maintenance**: Photovoltaic systems have low maintenance requirements after installation, which helps reduce long-term operational costs.

I.6.2. Disadvantages:

- **Sunlight Variability**: Solar energy depends on the availability of solar radiation, which leads to fluctuations and instability in photovoltaic power generation. Therefore, energy storage systems or hybrid integration with other energy sources are often required to ensure a continuous power supply.
- **High Initial Costs**: Despite the continuous decrease in the cost of solar energy technologies, the initial investment cost of installing photovoltaic systems remains relatively high.
- **Environmental Impact**: Although solar energy is considered a clean source during the operational phase, the manufacturing and disposal of solar panels may cause indirect environmental impacts.
- **Space Requirement**: Photovoltaic systems require relatively large areas, whether on rooftops or land, which may limit their deployment in densely populated urban areas or locations with limited space.
- **Dependency on Weather Conditions**: The performance of solar systems is affected by weather conditions such as clouds, rain, and snow, which leads to a temporary reduction in energy production efficiency.

I.7. Conclusion:

In conclusion, this chapter addressed the fundamental principles of solar radiation and photovoltaic energy conversion. It explained how solar cells utilize the photovoltaic effect to convert solar radiation into electrical energy. It also presented models and characteristics of photovoltaic generators, with a focus on key factors affecting their efficiency, such as temperature and load resistance.

In addition, the chapter discussed different types of photovoltaic cells according to the crystalline structure of silicon. It also outlined the main components of photovoltaic modules, highlighting the main advantages and disadvantages of photovoltaic solar energy technology.

Chapter II

DC-DC Converter

II.1. Introduction :

DC-DC converters are essential electronic circuits in modern power management systems, whose primary function is to convert a direct current (DC) voltage from one level to another while ensuring a stable and efficient power supply to various electronic devices and systems.

In practical applications, the input voltage may vary due to several factors, such as battery discharge over time or changes in load conditions. In this context, DC-DC converters regulate the output voltage and maintain it at a constant level, ensuring stable operation of system components.

These converters are characterized by high power conversion efficiency, as they rely on switching techniques that reduce energy losses associated with conventional devices such as linear regulators, which often dissipate energy in the form of heat. This results in improved overall system efficiency and extended battery life in portable applications.

In addition, DC-DC converters offer operational flexibility by enabling step-up or step-down voltage conversion according to system requirements, thereby improving power distribution management within electronic circuits. They can also provide galvanic isolation between the input and output stages, which reduces the effects of ground loops and protects sensitive components from voltage spikes and electrical noise.

II.2. DC-DC Converters :

DC-DC converters are static converters supplied by a direct current (DC) voltage source and are designed to produce an adjustable DC output voltage across an electrical load.

These converters can be designed using thyristors in high-power applications, where power levels can reach several hundred megawatts, with relatively low switching frequencies in the range of a few kilohertz.

In low- and medium-power applications, transistors are used in their construction, allowing operation at power levels of up to several hundred kilowatts, with high switching frequencies that can reach up to 100 kHz.

The figure below illustrates the standard symbol of a DC-DC converter.

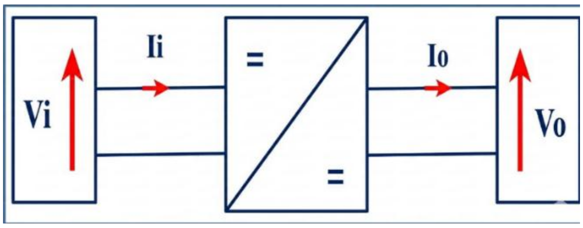

Figure II.1. DC-DC Converters

II.3. Applications of DC-DC Converter :

Switch-mode power converters have experienced widespread adoption in recent years across various domains of modern electronics, including industrial, commercial, utility, and consumer sectors. In the context of low-power DC–DC conversion applications, most energy conversion systems rely on three fundamental topologies: the buck converter, the boost converter, and the buck–boost converter. However, certain specialized applications necessitate the use of advanced topologies or modified versions of these conventional structures.

Despite the wide variety of DC–DC converters proposed in the literature, there is no single design capable of meeting the requirements of all applications, due to variations in operating conditions and system constraints. In general, power conversion techniques have gained significant importance owing to their extensive use in industry, scientific research, technological development, as well as in everyday applications [4].

DC–DC converters constitute a fundamental component in the field of power electronics and energy drive systems, given their crucial role in numerous industrial applications. Some of these applications are illustrated in Figure (II.2). In addition, high voltage gain converters are utilized in advanced applications such as radar systems, DC distribution networks, data centers, and renewable energy systems [5].

Their importance is particularly evident in renewable energy applications, where they enable the boosting of low voltage levels generated by renewable sources to values suitable for integration into distribution networks. Furthermore, DC distribution systems offer several advantages, including a reduction in the number of conversion stages, lower overall cost, and improved power quality, making them a preferred solution for a wide range of modern applications.

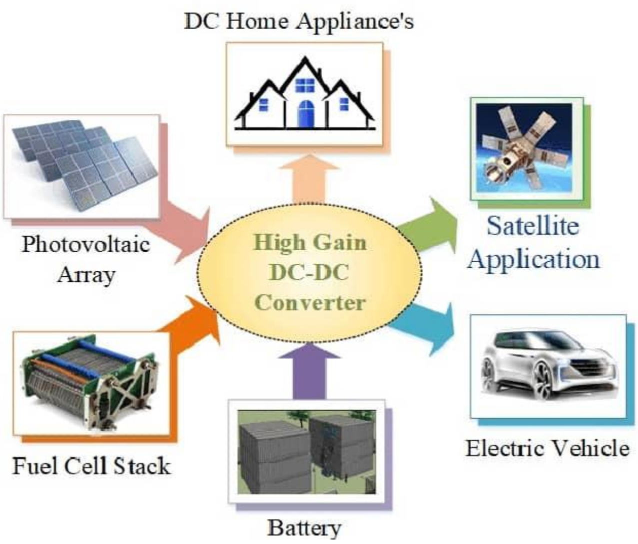

Figure II.2. Applications of DC/DC Converters.

The primary applications of DC-DC converter applications :

- **Renewable energy applications :** DC-DC converters used in renewable energy applications require drawing a DC input current that is as smooth and continuous as possible, in order to reduce ripple and improve signal quality. They should also be capable of integrating with various energy sources. In addition, non-isolated converters with interleaved operation and high voltage gain are often used to connect renewable energy sources to microgrids.
- **Medical devices :** Isolated DC-DC converters are essential in medical applications that require high safety levels, as they provide electrical isolation between the output side and hazardous input voltages. However, non-isolated converters can be used in certain applications, such as power supply systems for X-ray devices.
- **Vehicles :** Isolated DC-DC converters are essential in medical applications that require high safety levels, as they provide electrical isolation between the output side and hazardous input voltages. However, non-isolated converters can be used in certain applications, such as power supply systems for X-ray devices.
- **Smart lighting :** In the field of vehicles, the main DC-DC converter converts energy from the high-voltage battery into low DC voltages used to operate auxiliary systems such as lighting, windshield wipers, and window control systems. This applies to both electric and hybrid vehicles. Electrical isolation is also essential in cases where control circuits need to be separated from high-voltage areas. Buck-Boost converters are used for both step-up and step-down voltage regulation, while charge pump converters are used for polarity inversion.

II.4. Types of DC-DC converters :

There are three types of DC-DC converters, namely: Buck, Boost, and Buck-Boost.

II.4.1. Buck Converter :

Buck converter is a type of DC–DC converter used specifically to achieve step-down conversion of a DC input voltage to a lower output level. It converts a constant DC input voltage into a regulated DC output voltage, but with a magnitude lower than the input.

Thus, the main objective of this converter is to produce a lower DC output voltage compared to the applied input voltage.

It is also known by several other names, such as: Step-down DC–DC converter, Step-down chopper, or Buck regulator.

II.4.1.1 Operating Principle of Buck Converter :

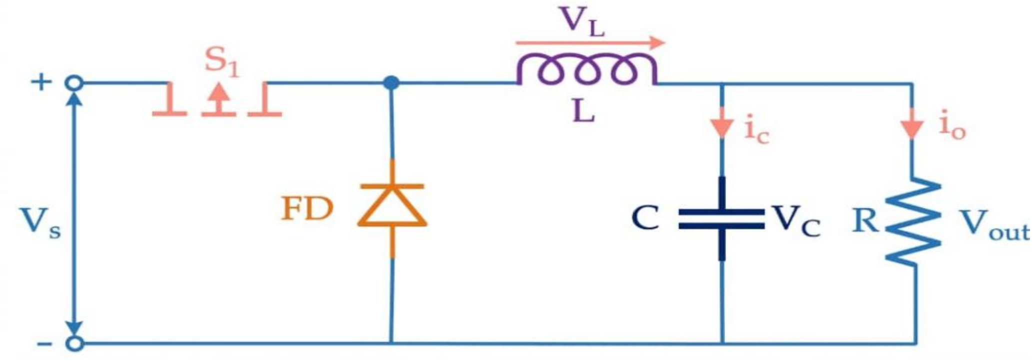

Figure II.3. The Circuit Representation of Buck Converter

The previous figure shows that the circuit is not limited to a single power electronics device acting as the main switch; it also includes a freewheeling diode, which operates as a secondary switching element in the configuration. The combination of these two components forms a structure associated with a low-pass LC filter, which is primarily used to reduce voltage and current ripples. This results in a more stable and well-regulated DC output. A resistive load is also connected across this arrangement to represent the electrical load of the circuit.

The circuit operates in two main modes. The first mode corresponds to the condition in which the power MOSFET switch S1 is in the ON state.

In this condition, switch S1 is closed, allowing current to flow through it and enabling continuous energy transfer within the circuit.

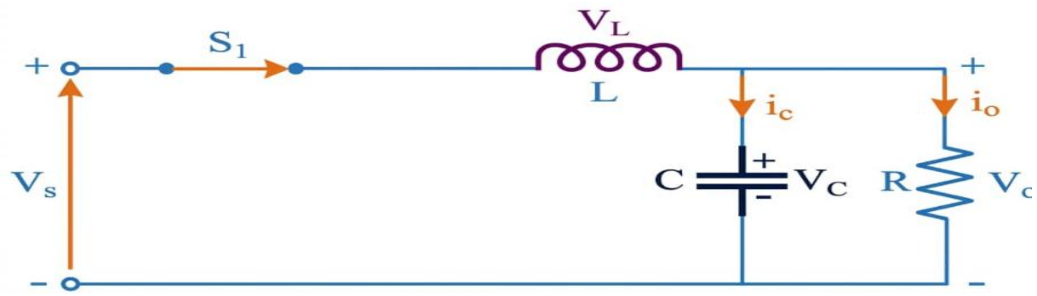

Figure II.4. Buck Converter When S1 is Closed

Initially, when a constant DC voltage is applied to the input terminals of the circuit with switch S_1 in the ON state, current flows through the circuit along the path described previously. As a result of this current, the inductor stores energy in the form of a magnetic field.

In parallel, current also flows through the capacitor, causing it to store electrical charge. Consequently, the voltage across the capacitor appears at the load terminals.

However, the inductor obeys Lenz's law, which states that the energy stored in it generates an electromotive force that opposes the cause producing it. This results in an induced current and a reversal of the voltage polarity across the inductor.

Here the total time period is a combination of T_{on} and T_{off} time.

$$T = T_{on} + T_{off} \tag{II. 1}$$

The duty cycle is written as:

$$D = \frac{T_{on}}{T} \tag{II. 2}$$

On applying KVL, in the above-given circuit

$$V_s = V_L + V_{\text{out}} \tag{II. 3}$$

$$V_L = V_s - V_{\text{out}} \tag{II. 4}$$

Also,

$$V_L = L\frac{di_L}{dt} = V_s - V_{\text{out}} \tag{II. 5}$$

$$\frac{di_L}{dt} = \frac{V_s - V_{out}}{L} \tag{II. 6}$$

When S1 is in closed condition then T_{on} = DT thus Δt = DT. Therefore, we can write

$$\frac{\Delta i_L}{\Delta t} = \frac{V_s - V_{\text{out}}}{L} \tag{II. 7}$$

$$\frac{\Delta i_L}{DT} = \frac{V_s - V_{\text{out}}}{L} \tag{II. 8}$$

Hence,

$$\Delta i_t = \left(\frac{V_s - V_{\text{out}}}{L}\right) DT \tag{II. 9}$$

The above equation represents the change in current through the circuit when switch S1 is closed.

The second operating mode occurs when switch S_1 is turned OFF and switch S_2 is turned ON. The automatic activation mechanism of switch S_2 is governed by; however, this behavior is directly related to the operation of the inductor in the circuit. The inductor stores energy during the ON state of switch S_1, and once S_1 is opened, the inductor begins to act as a source of energy.

In this condition, the inductor releases the energy stored during the previous stage. Due to the reversal of voltage polarity across the inductor, the freewheeling diode becomes forward-biased, whereas it was previously reverse-biased as a result of the applied DC input voltage.

Due to this, the flow of current takes place in a way as shown in Figure (II.5):

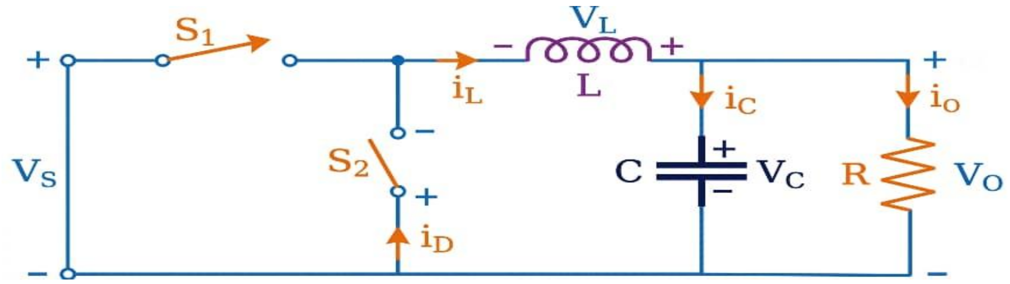

Figure II.5. Buck Converter When S2 is Closed

The current continues to flow in this condition until the energy stored in the inductor is completely depleted. Once the inductor is fully discharged, the diode enters a reverse-biased state (Reverse Bias), which results in the interruption of the current path through it.

Accordingly, switch S_2 is turned OFF while switch S_1 is simultaneously turned ON, initiating a new operating cycle. This process then continues periodically in a repetitive manner according to the operating mode of the circuit.

Applying KVL, in the Figure II.5:

$$0 = V_L + V_{\text{out}} \tag{II.10}$$

$$V_L = L\frac{di_L}{dt} = -V_{\text{out}} \tag{II.11}$$

Given that

$$\mathrm{T} = \mathrm{T_{on}} + \mathrm{T_{off}} \tag{II.12}$$

$$\mathrm{T} = \mathrm{DT} + \mathrm{T_{off}} \tag{II.13}$$

$$\mathrm{T_{off}} = \mathrm{T} - \mathrm{DT} \tag{II.14}$$

$$\mathrm{T_{off}} = (1 - \mathrm{D})\mathrm{T} \tag{II.15}$$

$$V_L = L\frac{\Delta i_L}{\Delta t} = -V_{\text{out}} \tag{II.16}$$

$$\mathrm{T_{off}} = \Delta \mathrm{t} = (1 - \mathrm{D})\mathrm{T} \tag{II.17}$$

$$L\frac{\Delta i_L}{(1 - D)T} = -V_{\text{out}} \tag{II.18}$$

So,

$$\Delta i_L = -\frac{V_{\text{out}}}{L}(1-D)T \tag{II.19}$$

This equation represents the rate of change in current through the inductor when the switch S1 is open.

It is widely recognized that the net change of current through the inductor in one complete cycle is zero. Thus,

$$\Delta i_{L(s1-closed)} + \Delta i_{L(S1-\text{ open })} = 0 \tag{II.20}$$

$$\frac{V_s - V_{\text{out}}}{L} DT + \left\{-\frac{V_{\text{out}}}{L}(1-D)T\right\} = 0 \tag{II.21}$$

On simplifying,

$$\frac{V_s DT}{L} - \frac{V_{\text{out}} DT}{L} - \frac{V_{\text{out}} T}{L} + \frac{V_{\text{out}} DT}{L} = 0 \tag{II.22}$$

$$\left(\frac{V_s DT}{L}\right) = \frac{V_{\text{out}} T}{L} \tag{II.23}$$

$$V_{\text{out}} = DV_s \tag{II.24}$$

The figure (II.6) illustrates represents the waveform representation of Buck Converter:

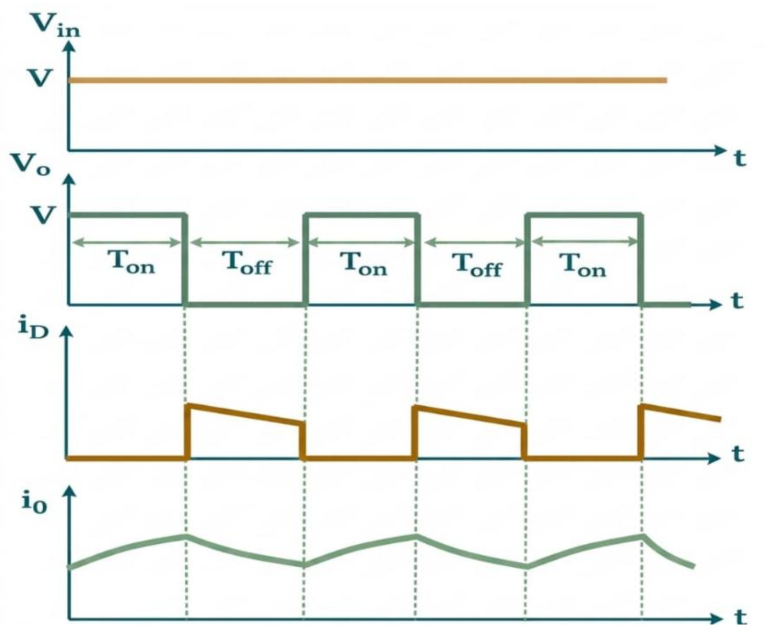

Figure II.6. Waveform Representation

Consequently, it can be concluded that buck converters are used to provide a lower value of dc signal from a fixed dc input.

II.4.2. Boost Converter :

Boost converters, also known as step-up DC–DC converters, are a type of chopper circuit used to increase the output voltage to a level higher than the applied input voltage.

In this type of converter, DC-to-DC conversion is performed in a way that produces an output voltage greater than the source voltage. The name “Boost” is given because the output voltage is effectively raised (or amplified) compared to the input voltage.

II.4.2.1 Operating Principle of Boost Converter :

The figure (II.7) illustrates the circuit representation of the boost converter:

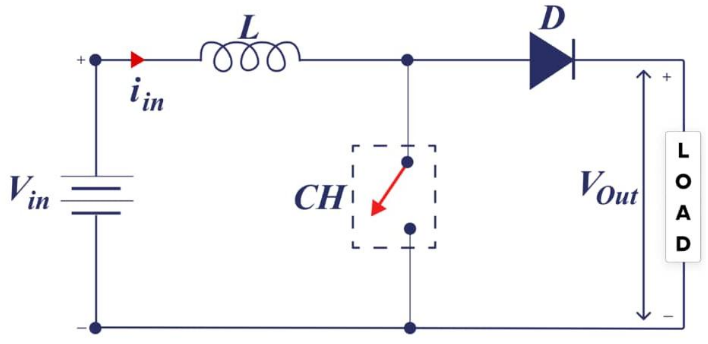

Figure II.7. Elementary Circuit of Boost Converter

This circuit represents the basic form of a Step-Up DC–DC Converter, which primarily relies on the presence of a large inductor L connected in series with the voltage source. This circuit configuration is designed to achieve a regulated DC output by controlling the switching operation within the circuit.

To explain the operating principle for obtaining a higher DC voltage at the load, when the electronic switch (Chopper CH) is in the ON state and a DC supply is applied, current begins to flow through the closed path of the circuit, initially passing through the inductor as shown in the figure.

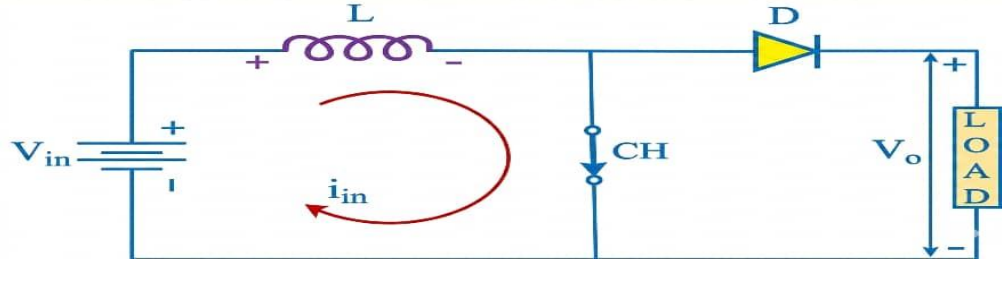

Figure II.8. The Chopper CH is in on State

of the current flowing in the circuit. Meanwhile, the diode is in a reverse-biased condition, which prevents it from conducting and thus blocks current flow through that branch of the circuit during the ON state of the DC–DC converter.

As a result, the total output voltage of the converter appears across the load terminals, thereby supplying the required voltage to the load during this operating stage.

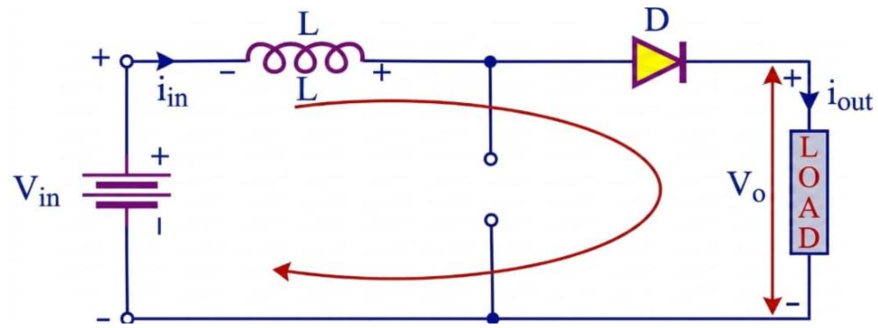

Figure II.9. The Chopper CH is in Off State

When switch CH transitions to the OFF state, the current path that was conducting during the ON state is immediately interrupted. However, due to the inherent property of the inductor (Inductor) to store energy in the form of a magnetic field, the current does not cease instantaneously at the moment of switching.

According to Lenz's law, an induced current is generated that opposes the change causing it. This results in a reversal of the voltage polarity across the inductor. Consequently, the diode becomes forward-biased (Forward Bias), providing an alternative path for the current to flow through the diode toward the load during the OFF interval (Toff).

Nevertheless, it should be noted that the inductor current exhibits a decreasing behavior over time, gradually diminishing until it eventually becomes zero due to the depletion of the energy stored in the magnetic field.

Thus, the total voltage across the load will be given as:

$$V_{\text{out}} = V_{\text{in}} + V_L \quad \text{(II. 25)}$$

This means that the output voltage becomes higher than the applied input voltage, indicating that the converter performs a step-up conversion. This occurs due to the inductor storing energy during the T_{On} interval and then releasing this energy during the T_{off} interval, which results in an increased output voltage compared to the input voltage.

During the T_{on} period, the voltage across the inductor will be given as:

$$V_L = L\frac{di}{dt} \quad \text{(II. 26)}$$

Figure (II.10) illustrates the waveform representation of the step-up chopper shown below:

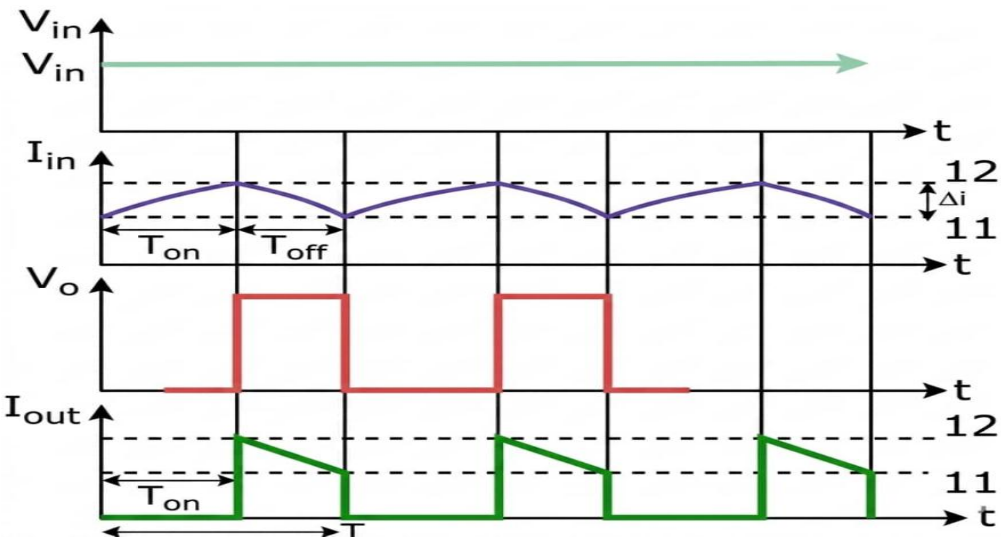

Figure II.10. Waveform Representation

During the T_1 period, the current flowing through the inductor changes from i_1 to i_2, as previously illustrated. In contrast, during the T_{off} period, the inductor current returns from i_2 to i_1.

Regarding the voltage, during the turn-on period, the voltage across the inductor is equal to the supply voltage. This reflects the direct application of the input voltage across the circuit elements during this interval. But when CH gets off then on applying KVL in the figure shown above, we will get :

$$V_L - V_0 + V_{\text{in}} = 0 \quad \textbf{(II.27)}$$

This means :

$$V_L = V_0 - V_{\text{in}} \quad \textbf{(II.28)}$$

Considering that output current is varying linearly, the energy input provided by the source to the inductor, when CH is on, is given as:

$$W_{on} = (\text{ voltage across the inductor })(\text{ average current through the inductor })T_{\text{on}}$$

$$W_{on} = V_{\text{in}}\left(\frac{i_1 + i_2}{2}\right)T_{on} \quad \textbf{(II.29)}$$

Further, the energy that the inductor releases to the load when CH is off is given as:

$W_{\text{off}} =$ (voltage across the inductor) (average current through the inductor) T_{off}

$$W_{\text{off}} = V_{\text{out}} - V_{\text{in}} \left(\frac{i_1 + i_2}{2}\right) T_{\text{off}} \tag{II.30}$$

For a lossless system, comparing the two energies, we will have,

$$V_{\text{in}} \left(\frac{i_1 + i_2}{2}\right) T_{\text{on}} = V_{\text{out}} - V_{\text{in}} \left(\frac{i_1 + i_2}{2}\right) T_{\text{off}} \tag{II.31}$$

On simplifying,

$$V_{\text{in}} T_{\text{on}} = V_{\text{out}} T_{\text{off}} - V_{\text{in}} T_{\text{off}} \tag{II.32}$$

$$V_{\text{out}} T_{\text{off}} = V_{\text{in}} T_{\text{on}} + V_{\text{in}} T_{\text{off}} \tag{II.33}$$

$$V_{\text{out}} T_{\text{off}} = V_{\text{in}} (T_{\text{on}} + T_{\text{off}}) \tag{II.34}$$

Given that, $T = T_{on} + T_{off}$, therefore,

$$V_{\text{out}} T_{\text{off}} = V_{\text{in}} T \tag{II.35}$$

$$V_{\text{out}} = V_{\text{in}} \frac{T}{T_{\text{off}}} \tag{II.36}$$

$$V_{\text{out}} = V_{\text{in}} \frac{T}{T - T_{\text{on}}} \tag{II.37}$$

$$V_{\text{out}} = V_{\text{in}} \frac{1}{\left(\frac{T}{T} - \frac{T_{\text{on}}}{T}\right)} \tag{II.38}$$

Given that , duty cycle i.e., $\alpha = T_{on}/ T$

$$V_{0ut} = V_{\text{in}} \frac{1}{(1 - \alpha)} \tag{II.39}$$

Thus, we can conclude here that the average load voltage can be stepped up with the change in the duty cycle.

II.4.3. Buck-Boost Converter :

The Buck–Boost converter is a type of DC–DC converter characterized by its ability to produce an output voltage that can be either higher or lower than the input voltage, depending on the operating conditions and duty cycle.

This converter is used to perform both step-up and step-down operations, functioning in a manner similar to transformers in AC circuits, but within a DC environment. It can also be considered equivalent to a flyback converter when a single inductor is used instead of a transformer.

Buck–Boost converters belong to the class of DC–DC converters known as choppers, and they are considered among the most versatile types due to their ability to provide a wide range of output voltage levels.. This converter can function as either a step-down or step-up converter, depending on its duty cycle, denoted as DA typical Buck-Boost converter circuit is shown below:

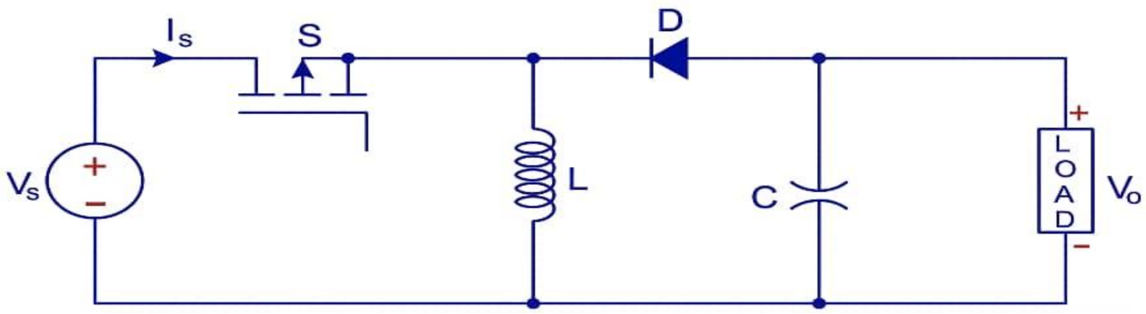

Figure II.11. The Circuit Representation of Buck-Boost Converter

The input voltage source is connected to a solid-state device that functions as the main control switch in the circuit. A diode is used as a secondary switch, connected in opposition to the direction of power flow from the source. This diode is linked to both the capacitor and the load, which are connected in parallel according to the given configuration.

The controlled switch operates using Pulse Width Modulation (PWM), which is employed to regulate the ON and OFF states. This technique can be implemented based on either time or frequency; however, the time-based approach is more commonly used in DC–DC converter applications.

Although frequency-based modulation offers a degree of flexibility, it requires a wide range of frequencies to achieve precise switching control, making it less practical. In contrast, time-based modulation is simpler and easier to implement, as the switching frequency remains constant while control is achieved by varying the conduction time.

The Buck–Boost converter operates in two main modes. The first mode occurs when the switch is in the ON state, allowing current to flow through the circuit elements.

Mode I: Switch is ON, Diode is OFF

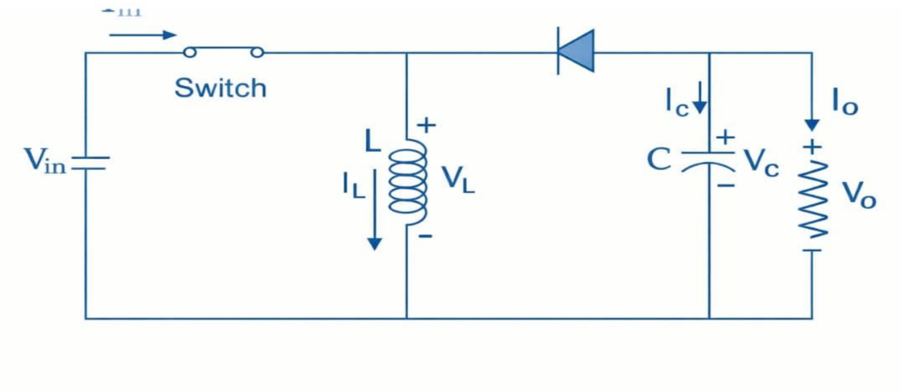

Figure II.12. The Equivalent Circuit of Mode Ⅰ

When the switch is in the ON state, it ideally represents a short circuit with negligible resistance, allowing current to flow without obstruction. As a result, the current flows through the switch and then through the inductor, before returning to the DC source.

During this interval, the inductor stores energy in the form of a magnetic field. When the switch transitions to the OFF state, the polarity of the voltage across the inductor reverses, enabling the current to continue flowing through the load and the diode, and then back to the inductor. Thus, the direction of current through the inductor remains unchanged despite the switching operation in the circuit.

The switch is on for a time T_{ON} and is off for a time T_{OFF}.

We define the time period, T, as:

$$T = T_{ON} + T_{OFF} \tag{II.40}$$

and the switching frequency:

$$f_{\text{switching}} = \frac{1}{T} \tag{II.41}$$

define another term, the duty cycle:

$$D = \frac{T_{ON}}{T} \tag{II.42}$$

This section analyses the Buck Boost converter in steady state operation for this mode using KVL.

$$V_{in} = V_L$$
$$V_L = L\frac{di_L}{dt} = V_{in}$$
$$\frac{di_L}{dt} = \frac{\Delta i_L}{\Delta t} = \frac{\Delta i_L}{DT} = \frac{V_{\text{in}}}{L} \quad \textbf{(II. 43)}$$

Since the switch is closed for a time T_{ON} = DT we can say that Δt = DT.

$$(\Delta i_L)_{\text{closed}} = \left(\frac{V_{in}}{L}\right) DT \quad \textbf{(II. 44)}$$

While performing the analysis of the Buck-Boost converter it should be noted that:

- The inductor current is continuous, and this behavior is achieved by selecting an appropriate value of the inductor L, which ensures continuous current flow and reduces ripples in the circuit.
- In the steady-state condition, the inductor current increases during the ON state from an initial value with a positive rate of change until it reaches its maximum value. It then decreases during the OFF state with a negative slope, returning to its initial value. Consequently, the net change in the inductor current over a complete switching cycle is equal to zero.

Mode II: Switch is OFF, Diode is ON

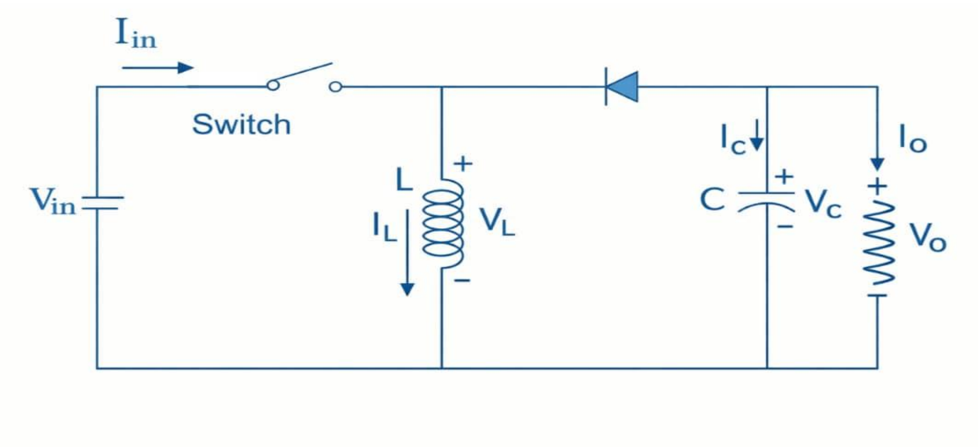

Figure II.13. The Equivalent Circuit of Mode II

In this condition, the polarity of the inductor is reversed, leading to the release of the energy stored within it. This energy is then transferred and dissipated across the load resistance. As a result, the current continues to flow in the same direction through the load, while the output voltage is increased, since the inductor effectively acts as an additional energy source in parallel with the input supply.

However, for analytical purposes, the original conventions are maintained in order to analyze the circuit using Kirchhoff's Voltage Law (KVL).

Buck Boost Converter Formula

The Buck Boost converter analyses in steady state operation for Mode II using KVL.

$$V_L = V_o \quad \textbf{(II.45)}$$

$$V_L = L\frac{di_L}{dt} = V_o \quad \textbf{(II.46)}$$

$$\frac{di_L}{dt} = \frac{\Delta i_L}{\Delta t} = \frac{\Delta i_L}{(1-D)T} = \frac{V_o}{L} \quad \textbf{(II.47)}$$

Since the switch is open for a time

$$T_{OFF} = T - T_{ON} = T - DT = (1-D)T \quad \textbf{(II.48)}$$

it can be concluded that

$$\Delta t = (1-D)T \quad \textbf{(II.49)}$$

$$(\Delta i_L)_{\text{open}} = \left(\frac{V_o}{L}\right)(1-D)T \quad \textbf{(II.50)}$$

It is already established that the net change of the inductor current over any one complete cycle is zero.

$$(\Delta i_L)_{\text{closed}} + (\Delta i_L)_{\text{open}} = 0 \quad \textbf{(II.51)}$$

$$\left(\frac{V_o}{L}\right)(1-D)T + \left(\frac{V_{\text{in}}}{L}\right)DT = 0 \quad \textbf{(II.52)}$$

$$\frac{V_o}{V_{\text{in}}} = \frac{-D}{1-D} \quad \textbf{(II.53)}$$

The duty cycle D ranges between 0 and 1. When D exceeds 0.5, the output voltage becomes greater than the input voltage, whereas when D is less than 0.5, the output voltage becomes lower than the input voltage. In the special case where D = 0.5, the output voltage is exactly equal to the input voltage[8].

II.5. Comparison of Converter Types :

Table (II.1) presents the voltage gain and switch stress for the different converter topologies, and illustrates the evolution of voltage gain as a function of the duty cycle. Although several topologies can be classified as boost converters—particularly when the duty cycle exceeds 0.5—the conventional boost converter is the only one capable of providing voltage boosting over the entire duty cycle range.

For instance, at a duty cycle of 0.5, the boost converter produces an output voltage equal to twice the input voltage, whereas other derived topologies yield an output voltage equal to the input voltage at the same duty cycle. These derived topologies only begin to approach the behavior of the conventional boost converter when the duty cycle approaches unity (1)[9].

Converter /Parameters	Voltage Gain $\frac{Vout}{Vin}$	Voltage Controls $V_{k,max} = \lvert Vd,max \rvert$	Current Controls $i_{k,max} = V_{d,max} = i_{d,max}$
Boost	$\frac{1}{1-\alpha}$	$\frac{Vin}{1-\alpha} + \frac{\Delta Vout}{2}$	$\frac{Iout}{1-\alpha} + \frac{\Delta IL}{2}$
Buck	$\frac{\alpha}{1-\alpha}$	$\frac{Vin}{1-\alpha} + \frac{\Delta Vout}{2}$	$\frac{VC}{1-\alpha} + \frac{\Delta Vout}{2}$
Buck-Boost	α	Vin	$i_L + \frac{\Delta IL}{2}$

Table II.1. Comparison of Converter Types.

II.6. Efficiency of Static Converters :

The table provides insight into the efficiency of some well-known converter types. [10]

Structure	Conversion Efficiency	Battery
Boost	92%	24V
Buck	93%	12V
Buck-Boost	92%	12-24V

Table II.2. Efficiency of Static Converters.

II.7. Conclusion :

In conclusion, DC-DC converters are considered fundamental components in modern electronic systems, as they contribute effectively to power management by converting electrical voltage levels to meet the requirements of various loads. These converters are characterized by their diverse topologies, such as the Buck, Boost, and Buck-Boost converters, which provide significant flexibility in addressing the varying voltage needs of electronic systems.

These converters have widespread applications across numerous vital sectors, including the automotive industry, renewable energy systems, telecommunications, and consumer electronics. They are used to power small electronic devices and play a pivotal role in regulating and managing energy flow within solar power systems, making them indispensable for achieving high efficiency and reliability.

Furthermore, Maximum Power Point Tracking (MPPT) is regarded as a cornerstone technology in renewable energy systems, particularly in photovoltaic (PV) applications. This technique enables the extraction of maximum power from solar panels by adjusting the electrical operating point to ensure operation at the maximum power level. In the following chapter, this technology will be discussed in greater detail, highlighting its importance and reviewing the main implementation methods.

Chapter III

Maximum Power Point Tracking

III.1. Introduction :

To address the issue of low performance in solar panels and achieve maximum possible efficiency, it is necessary to comprehensively optimize the design of all components of the photovoltaic (PV) system. It is also essential to improve the DC/DC converters that act as an interface between the solar generator and the load, with the aim of continuously extracting maximum power. This is accomplished by operating the system at the Maximum Power Point (MPP) without energy transfer losses, using Maximum Power Point Tracking (MPPT) techniques. This approach ensures the extraction of the highest possible power despite continuous variations in operating conditions, such as solar irradiance and temperature.

MPPT control techniques have undergone significant development since the 1970s, starting with simple methods based on monitoring voltage and current, and evolving into more advanced and accurate algorithms for determining the maximum power point of PV systems. Among the most widely used techniques are the Incremental Conductance (INC) method, the Perturb and Observe (P&O) method, and the Hill Climbing method[11].

III.2. Maximum Power Point Tracking :

Improving the efficiency of photovoltaic (PV) systems requires maximizing the power extracted from the solar generator. This can be achieved by determining the optimal operating point that ensures effective matching between the load impedance and the voltage source. In this context, the DC-DC converter plays a fundamental role as an impedance adapter, ensuring operation at the optimal point and thereby enabling maximum power extraction from the PV generator[12].

From this perspective, maximizing the power generated by a photovoltaic source relies on the continuous search for the optimal operating point, a process known as Maximum Power Point Tracking (MPPT). This technique is based on iterative search algorithms aimed at identifying the operating point that yields the maximum possible power without compromising the stability and continuity of system operation.

The power extracted from the PV module is estimated based on voltage and current measurements, where power is calculated as the product of these two quantities. These measurements are utilized within various algorithms designed to accurately track the true Maximum Power Point (MPP).

Several MPPT techniques exist, including the constant voltage method, the constant current method, the Incremental Conductance algorithm, and the Perturb and Observe method. In this work, the Perturb and Observe method has been adopted due to its simplicity and ease of implementation compared to other approaches.

III.3. Working principle of MPPT :

Advanced control strategies exist to ensure that systems operate at the optimal points of their operational characteristics without requiring prior knowledge of these points, the timing of their variation, or the reasons behind such changes. In the context of energy sources, these optimal points correspond to what is known as the Maximum Power Point (MPP). This type of control is widely referred to in the scientific literature as Maximum Power Point Tracking (MPPT) [13].

The operating principle of MPPT techniques is based on performing a dynamic and continuous search for the maximum power point while ensuring optimal matching between the generator and the load. This matching enables the transfer of the maximum available power and contributes significantly to improving system efficiency and overall performance, particularly under continuously varying environmental conditions such as solar irradiance and temperature.

To simplify the study and operation of this type of control system, a direct current (DC) load is typically employed. As illustrated in the power conversion chain, the MPPT control system is inherently associated with a four-pole element (also known as a Two-Port Network) that provides the necessary degrees of freedom to achieve electrical adaptation between the photovoltaic generator and the load.

In solar energy conversion applications, this four-pole element is practically implemented using a DC-DC converter. This converter enables the adjustment of the photovoltaic generator's operating point so that the power it delivers corresponds to the maximum power (PMAX) it can generate. Consequently, this maximum power can be efficiently transferred to the load, thereby enhancing the overall performance of the photovoltaic system.

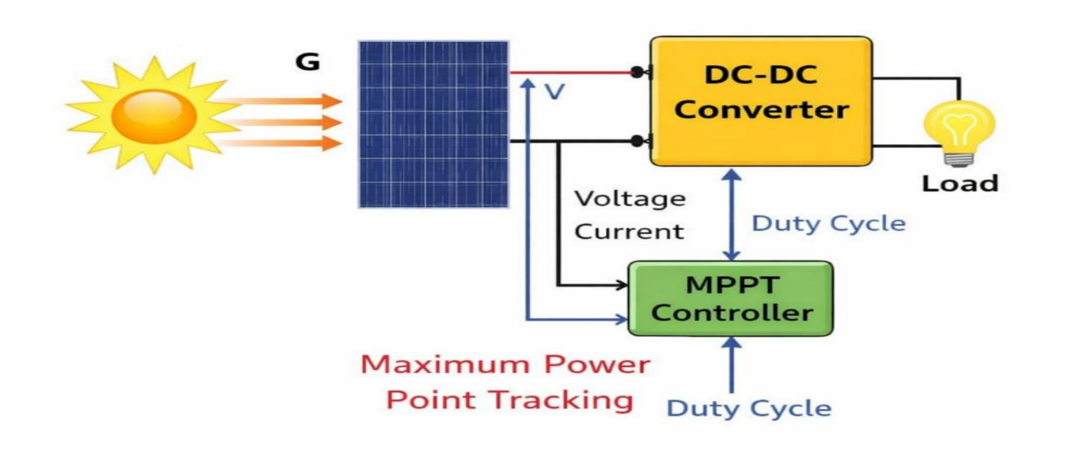

Figure Ⅲ.1. Block Diagram of The PV System

The most commonly used control technique is based on automatically adjusting the duty cycle in order to drive the system toward its optimal operating point, especially under sudden load variations that may occur at any time. Figure (III.2) illustrates three (03) types of disturbances.

Depending on the type of disturbance, the operating point shifts from the first maximum power point (MPP1) to a new operating point (P1), which may be either close to or far from the optimal point. In the case of solar irradiance variation (case a), the duty cycle is adjusted in order to track and reach the new maximum power point (MPP2).

In the case of load variation (case b), the operating point also changes; however, the control system is able to re-establish a new optimal operating point through its control mechanism. To a lesser extent, changes in the operating point may also occur due to variations in the operating temperature of the photovoltaic module (case c).

Although control action is required in all cases, the required response time differs, being more critical and faster in the cases of irradiance and load variations compared to temperature variations[14].

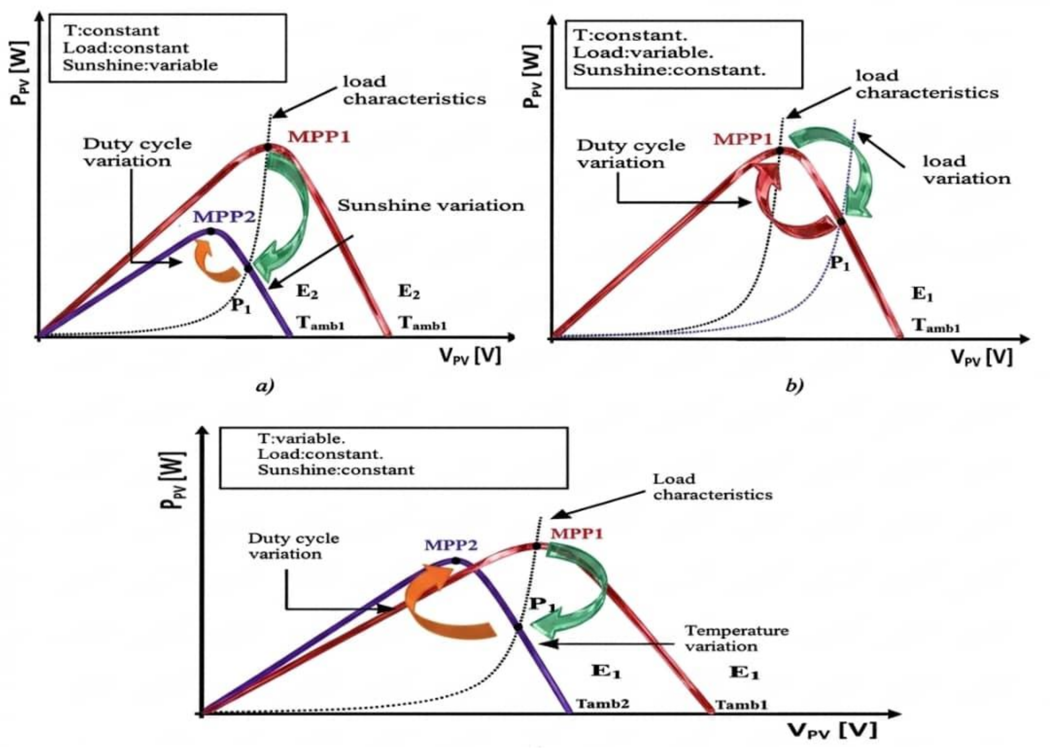

Figure Ⅲ.2. Search and Recovery Of MPP

III.4. Classification of MPPT Control :

MPPT (Maximum Power Point Tracking) controllers can generally be classified, according to the nature of their electronic implementation, into three main types: analog, digital, and hybrid systems that combine both approaches. However, a classification based on the search algorithm employed by the controller to determine the maximum power point, as well as the input parameters used in this process, is considered more significant from both scientific and practical perspectives, as it provides a deeper understanding of the performance and operational characteristics of these controllers.

III.4.1 Classification of MPPT Controllers Based on Input Parameters :

III.4.1.1. MPPT Controllers Operating from Input Parameters :

There are several types of Maximum Power Point Tracking (MPPT) controllers that operate based on analyzing variations in the power generated by the photovoltaic (PV) array in order to determine the optimal operating point. Among the most prominent of these methods are the Perturb and Observe technique and Incremental Conductance algorithms, where the extracted power value from the PV array is utilized to implement an appropriate control action that ensures efficient tracking of the maximum power point. This category also includes controllers based on proportional relationships between the optimal parameters of the maximum power point (Vopt and Iopt) and the characteristic parameters of the PV module (Voc and Isc).

Furthermore, controllers based on neural networks fall within this classification, as they rely either on large computer memory systems to store various possible operating conditions or on approximate models to simulate system behavior. In general, these controllers are characterized by high accuracy and fast response times, making them well-suited for applications requiring advanced dynamic performance[15].

III.4.1.2. MPPT Controllers Operating from Output Parameters of the Converter :

The scientific literature indicates the existence of a class of Maximum Power Point Tracking (MPPT) algorithms that rely on the output parameters of DC-DC converters. Among these are algorithms based on maximizing the output current, which are primarily employed in systems where the load is a battery. In such systems, the maximum power (Pmax) is estimated indirectly through the efficiency of the power converter; the higher the conversion efficiency, the more accurate this estimation becomes.

However, single-sensor-based systems inherently suffer from limited accuracy due to their reliance on partial information about the system’s state. It is also worth noting that many of these approaches were originally developed to meet the requirements of space applications, where constraints on complexity and resource availability play a critical role in control system design[15].

III.4.2. Classification of MPPT Controllers According to the Type of Search :

III.4.2.1. Indirect MPPT :

This type of Maximum Power Point Tracking (MPPT) algorithms relies on exploiting the relationship between measured variables, such as the open-circuit voltage (Voc), which can be easily determined in practice, and the approximate location of the maximum power point. This category also includes controllers that estimate the operating point of the photovoltaic system based on predefined parametric models.

Furthermore, this class encompasses methods that achieve optimal voltage tracking by relying solely on variations in the temperature of photovoltaic cells, as measured by a sensor. These controllers are characterized by their structural simplicity and ease of implementation; however, they are generally used in low-cost and low-accuracy systems, particularly in environments with relatively stable climatic conditions[16].

III.4.2.2. Direct MPPT :

This type of Maximum Power Point Tracking (MPPT) algorithms is based on determining the optimal operating point (MPP) using real-time measurements of current, voltage, or power within the photovoltaic system, which enables it to adapt to dynamic and unpredictable operating conditions. These approaches generally rely on numerical search algorithms that allow continuous tracking of the maximum power point without interrupting system operation.

The operating principle involves applying gradual and periodic variations to the operating voltage while observing the resulting change in power. If the variation leads to an increase in power, the search continues in the same direction; otherwise, the direction is reversed. Consequently, the actual operating point stabilizes with small oscillations around the maximum power point. Advanced algorithms have been developed to preserve this principle while reducing estimation errors, which may arise due to rapid changes in solar irradiance that can lead to incorrect search direction decisions.

Determining the instantaneous power of the photovoltaic generator, which is essential for the tracking process, requires measuring both voltage and current and calculating their product. Other approaches are based on introducing small sinusoidal perturbations in the converter switching frequency to analyze the direct and alternating components of the voltage signal, thereby adjusting the operating point as close as possible to the maximum power point.

This class of controllers is characterized by high accuracy and fast response, making it suitable for applications requiring dynamic performance and high reliability[16].

III.5. Different MPPT Commands Synthesis :

The scientific literature indicates a growing interest in the study and development of Maximum Power Point Tracking (MPPT) algorithms since 1968, which marks the introduction of the first control law specifically designed for renewable energy applications, particularly photovoltaic systems. Given the significant expansion in the number of studies published in this field, there has been a need to organize these algorithms into systematic classifications based on their fundamental principles, in order to facilitate their understanding, performance analysis, and areas of application.

III.5.1. First MPPT Commands Types :

The algorithm used in the first Maximum Power Point Tracking (MPPT) system was relatively simple, which can be attributed to the limited capabilities of microcontrollers available at that time. Moreover, applications—particularly in the space field—were subject to fewer constraints regarding temperature variations and solar irradiance levels.

A.F. Boehringer introduced the first control law applied to a photovoltaic system, based on an adaptive control approach aimed at maintaining the system at its maximum power point (MPP). This principle is illustrated in Figure 3 and can be readily implemented using computer systems.

The operating mechanism relies on calculating the instantaneous power at time t_i by measuring both the current I_{pv} and the voltage V_{pv}, and then comparing it with the value recorded at the previous time $(t_{i-}\ 1)$. Based on this comparison, a new duty cycle is determined and applied to the static converter in order to adjust the operating point and ensure optimal tracking.

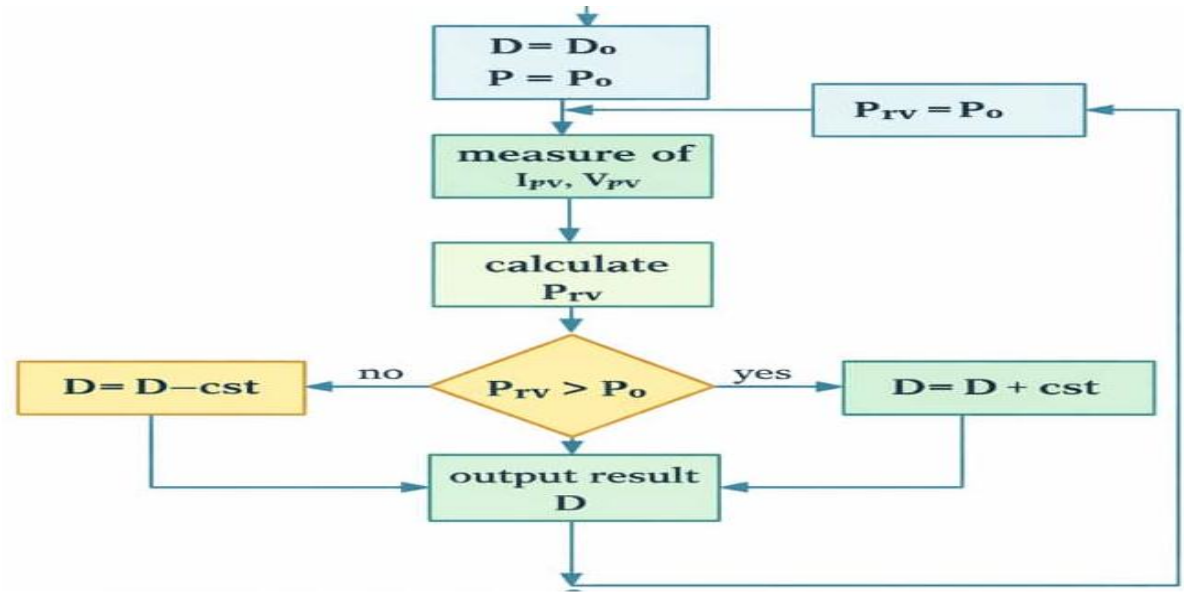

Figure Ⅲ.3. Bloc Diagram of a Digital MPPT Command

This principle remains theoretically valid and is currently implemented in more advanced and efficient numerical algorithms. These developments have significantly improved the response time as well as the accuracy of maximum power point (MPP) tracking, thereby enhancing the overall performance and effectiveness of tracking systems[14].

III.5.2. Efficient MPPT Commands Algorithms :

The four most commonly used methods in this field are, respectively: Hill Climbing, Perturb and Observe, Incremental Conductance, and Artificial Neural Networks.

These techniques are widely employed due to their effectiveness in optimizing performance and extracting optimal values in various systems.

III.5.2.1. Algorithm Perturb and Observe (P&O) :

The operating principle of the Perturb and Observe (P & O) Maximum Power Point Tracking (MPPT) algorithm is based on introducing a small variation in the photovoltaic voltage V_{pv} with low amplitude around its initial value, and then analyzing the effect of this variation on the resulting power P_{pv}.

Based on the analysis of the power behavior, as illustrated in Figure (Ⅲ.4), the position of the operating point relative to the Maximum Power Point (MPP) can be determined. If a positive change in voltage leads to an increase in power, this indicates that the operating point lies to the left of the MPP. Conversely, if the power decreases, this means that the operating point has exceeded the MPP.

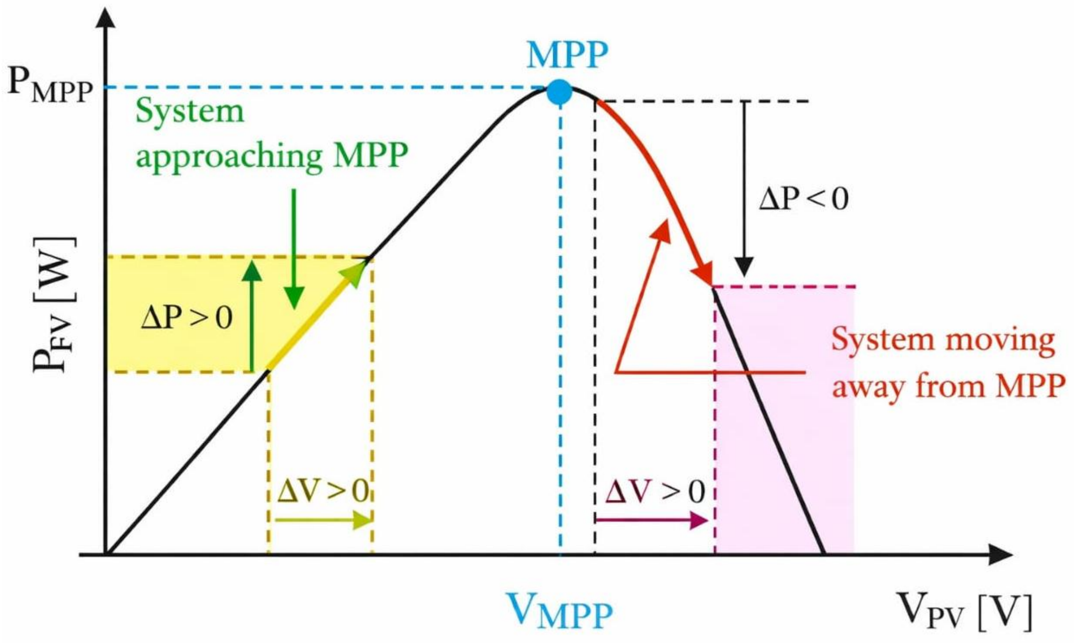

Figure Ⅲ.4. Ppv VS Vpv Characteristic of a Solar Panel

Figure (III.5) illustrates the algorithm associated with the conventional Maximum Power Point Tracking (MPPT) method based on the Perturb and Observe (P&O) approach, where the variation in power is analyzed after each perturbation applied to the system voltage.

This method relies on measuring both voltage and current using two sensors in order to calculate the photovoltaic generator power in real time and with good accuracy. It is considered one of the most widely used techniques in practical applications due to its simplicity and ease of implementation.

However, it has some limitations, the most important of which is the occurrence of oscillations around the Maximum Power Point (MPP) under steady-state conditions. This is due to the iterative nature of the search process for this point, which leads to continuous fluctuations of the operating point around the MPP.

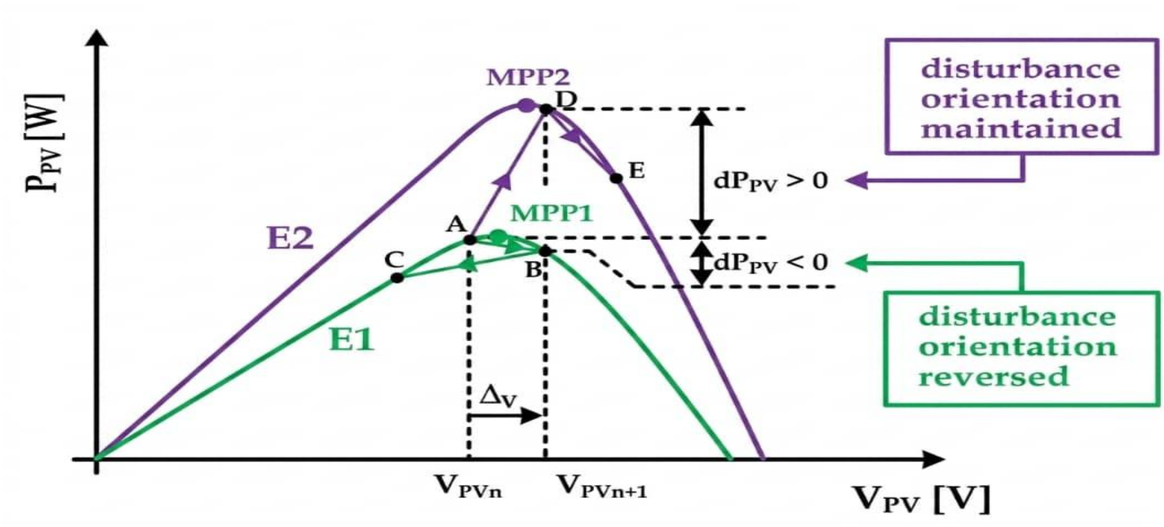

Figure Ⅲ.5. Divergence of The P & O Command Due to Radiation Variations

Figure (Ⅲ.6) shows a detailed algorithm of the P & O command.

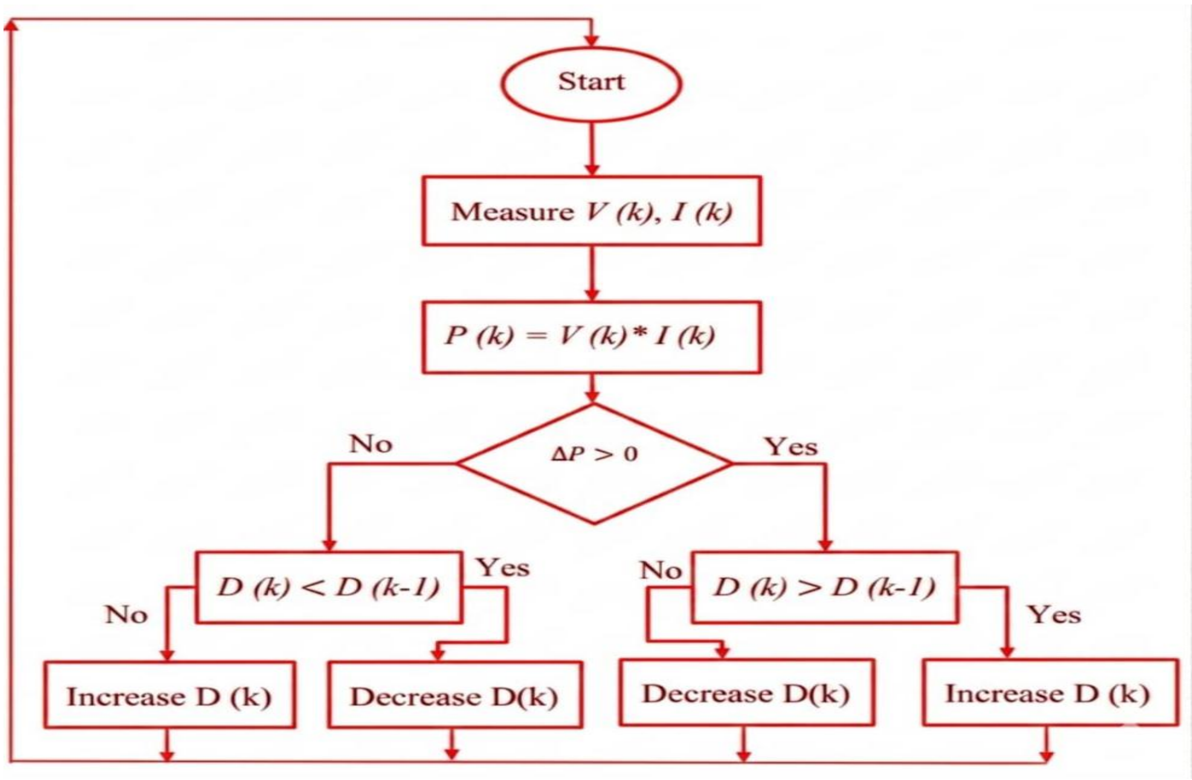

Figure Ⅲ.6. Algorithm of The P & O Type of Command

To understand this behavior, It is useful to consider a constant solar irradiation level E_1, where the initial operating point is located at point A. When a voltage perturbation of magnitude Δ V is applied, the operating point moves to point B, which reflects a change in the operating condition without any variation in the solar irradiation level.

As a result of detecting a negative sign of the power derivative, the direction of the perturbation is reversed. This leads, under steady-state conditions, to oscillations around the maximum power point (MPP), due to the continuous movement of the operating point between points B and C. These oscillations are a characteristic feature of the Perturb and Observe (P&O) method.

It is also important to note that power transfer losses vary in magnitude depending on the relative positions of points B and C with respect to point A, becoming more or less significant according to how far the operating point is from the MPP.

When the solar irradiation changes from E_1 to E_2, the operating point shifts from A to D, which is interpreted as an increase in the output power, i.e., a positive change in power[14].

III.5.2.2. Algorithm Hill Climbing :

The hill climbing maximum power point tracking (MPPT) method is characterized by its simplicity of implementation, as it uses the duty cycle of the boost converter as a feedback variable during the tracking process [17],[18].

However, this technique suffers from several drawbacks, the most important of which is the trade-off between system stability under constant solar irradiation conditions and the response speed to changes in environmental conditions. In addition, it exhibits poor dynamic performance under rapid variations in solar irradiance, which affects tracking accuracy [17],[18].

During periods of steady irradiance, the system requires a very small duty cycle variation ΔV in order to minimize oscillations around the maximum power point (MPP) and thus improve stability. However, this may lead to a reduction in the amount of energy extracted from the photovoltaic system.

On the other hand, under rapidly changing irradiance conditions, increasing the value of PV becomes necessary to speed up the tracking of the maximum power point and improve the response time, although this may result in increased oscillations around the optimal operating point.

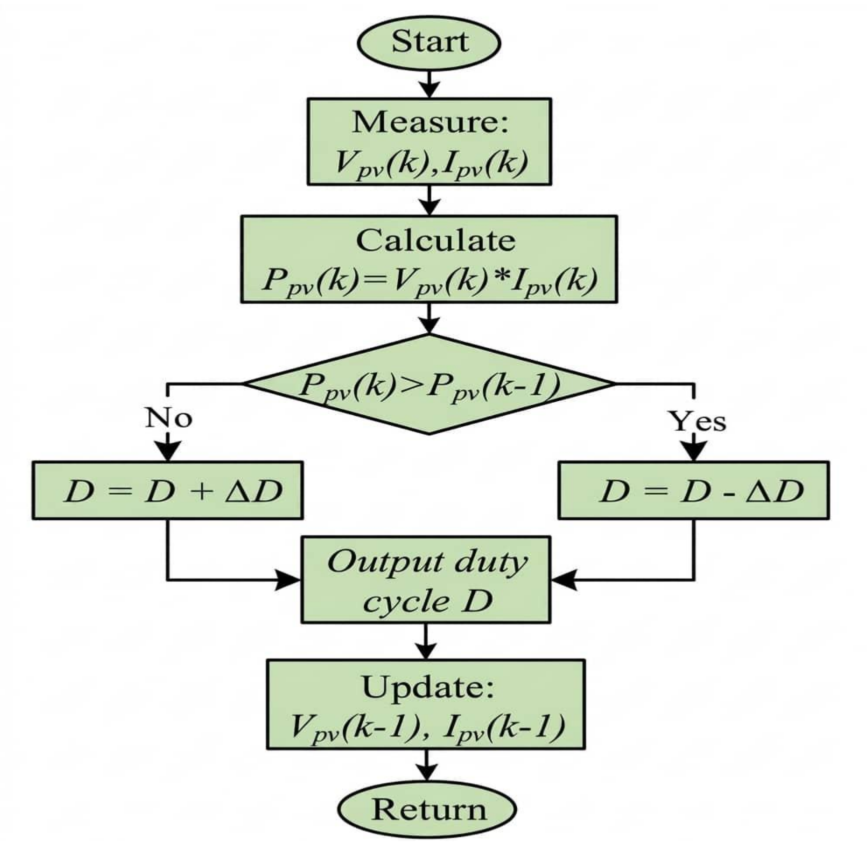

Figure Ⅲ.7. State Flowchart of Hill Climbing MPPT Technique

III.5.2.3. Algorithm Incremental conductance (INC) :

The principle of this algorithm is based on the use of the conductance value G =I/V and the conductance variation ΔG, in order to determine the position of the operating point relative to the maximum power point (MPP).

According to this principle, if the conductance variation ΔG is greater than the negative of the conductance (-G), the duty cycle is reduced. Conversely, if ΔG is less than (-G), the duty cycle is increased.

This process is repeated iteratively until the maximum power point (MPP) is reached [19].

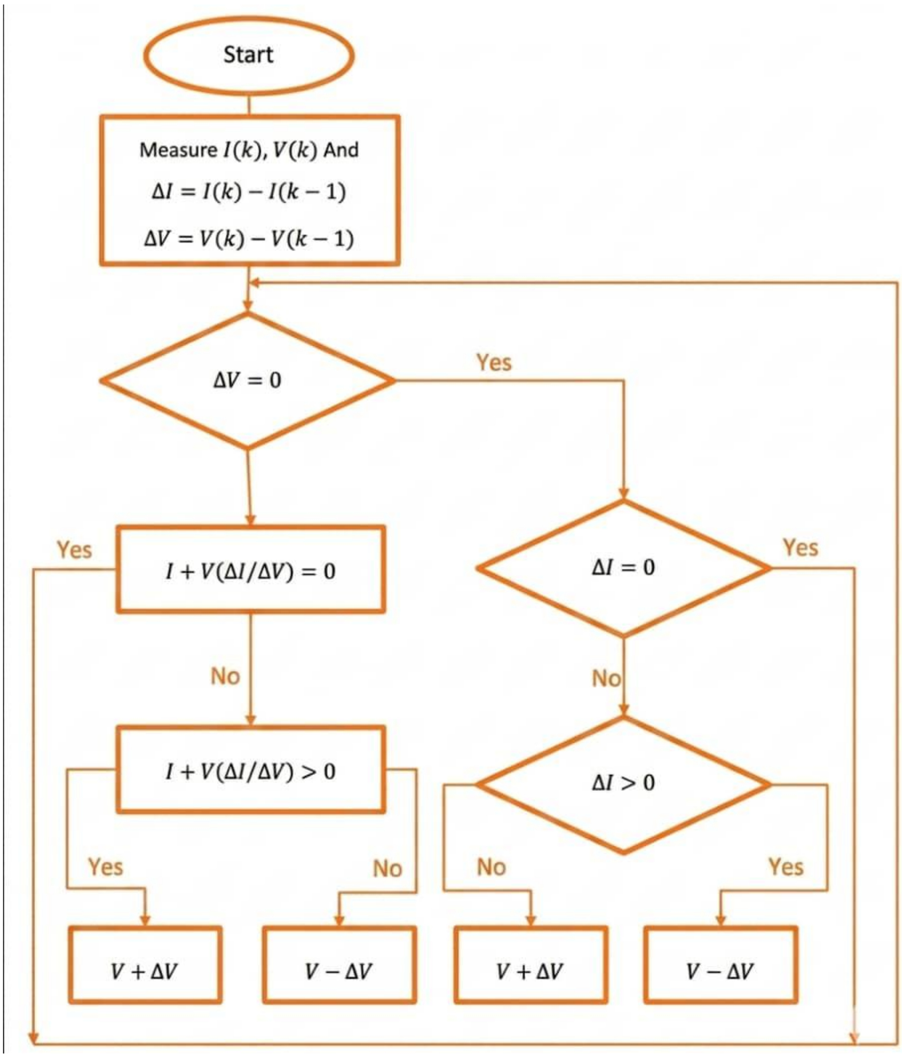

Figure Ⅲ.8. Flowchart for The Incremental Conductance Algorithm

III.5.2.4. Artificial Neural Networks (ANN) :

In general, artificial neural networks rely on a large number of computational units (processors) operating in parallel and organized into multiple layers. The first layer receives raw data inputs in a manner similar to how the visual nerves receive sensory information in living organisms.

Subsequently, each successive layer receives and further processes the outputs of the previous layer. This sequential processing resembles the biological nervous system, where neurons receive signals from other functionally connected neurons.

Finally, the last layer is responsible for producing the system's final outputs, which represent the overall result of the neural network's processing.

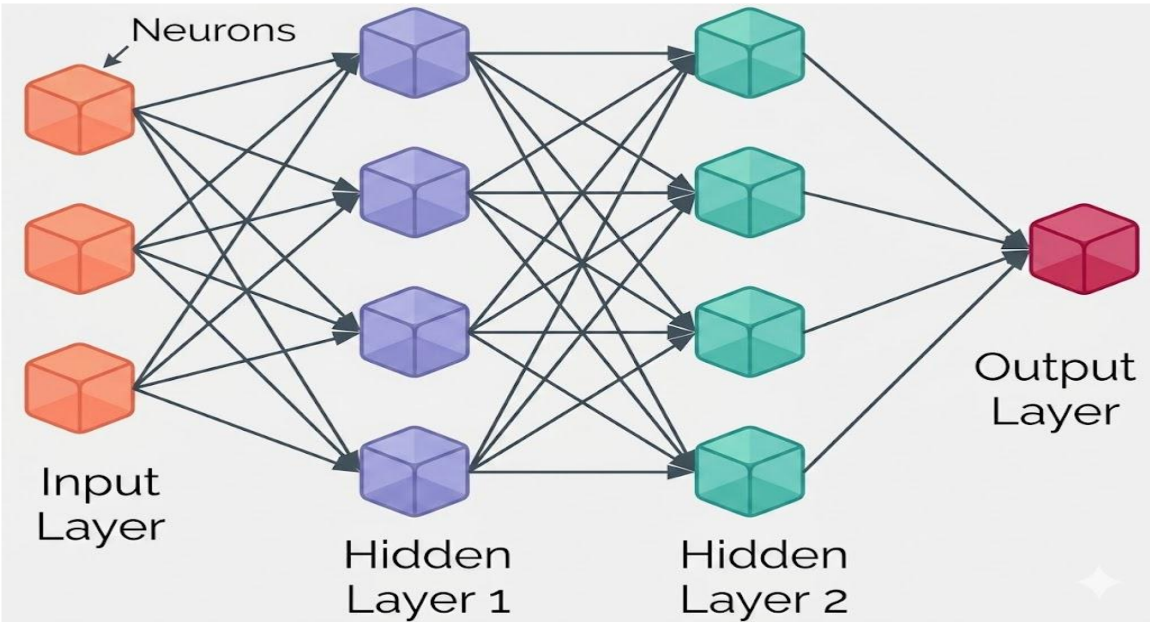

Figure Ⅲ.9. Functioning of Artificial Neural Networks

Neural networks enable computers to learn from new data using specialized algorithms. These systems are trained on labeled data in order to acquire the ability to perform tasks such as object recognition by analyzing patterns and relationships within the training data.

Unlike traditional algorithms, neural networks do not rely on direct programming to accomplish tasks; instead, they learn in an adaptive manner that closely resembles the way the human brain develops and learns during growth.

In general, learning methods in neural networks can be classified into three main types:

1. **Supervised Learning**: The algorithm is trained using labeled data, where its parameters are iteratively and continuously adjusted until it is able to produce the desired outputs with high accuracy.

2. **Unsupervised Learning :** The neural network processes unlabeled data, where the cost function serves as a guiding mechanism for the learning process toward the desired outcomes by measuring the deviation between the actual outputs and the target outputs.

3. **Reinforcement Learning :** The neural network is rewarded when it produces positive results and penalized when it produces negative results, which contributes to the gradual improvement of its performance over time. This learning approach is similar to the way humans learn through trial and error and by correcting their mistakes.

III.5.2.4.1. Application of Artificial Neural Networks in MPPT :

Artificial neural networks are employed to improve maximum power point tracking (MPPT), which is a key component in photovoltaic (PV) systems. These networks enhance the efficiency of solar energy harvesting by continuously adjusting the operating point of PV panels in order to maximize the output power.

This adjustment takes into account various environmental changes such as solar irradiance, temperature, and partial shading conditions. As a result, the use of neural network-based MPPT leads to a significant improvement in photovoltaic system performance and an increase in overall energy production.

This example highlights the practical application of artificial neural networks and their effective role in enhancing the performance of PV systems through improved maximum power point tracking algorithms [20].

III.5.2.4.2. Implementation of ANN in MATLAB/SIMULINK :

The Neural Network Fitting app in MATLAB provides an interactive and user-friendly environment for designing, training, and evaluating artificial neural networks. The process includes selecting the dataset, defining the network architecture, performing the training procedure, and analyzing the results using various plots and statistical performance metrics.

This application is widely used in many engineering fields, particularly in maximum power point tracking (MPPT) systems, due to its ability to accurately and effectively model complex nonlinear relationships between input and output variables.

1. **Data Collection :**

   The first stage of the proposed method consists of collecting data generated from simulations of maximum power point tracking (MPPT) algorithms under various operating conditions. Data collection is a fundamental and crucial step in developing the artificial neural network (ANN) model, as it is later used for training and evaluation to ensure the accuracy and effectiveness of the model [20].

2. **Setting Up the Neural Network Fitting Tool :**

To begin the implementation process, the Neural Network Fitting tool in MATLAB is opened. This tool provides an interactive and simplified interface for designing, training, and evaluating artificial neural networks. The predefined variables are then imported, and the tool is configured and adjusted according to the requirements of the target application [21].

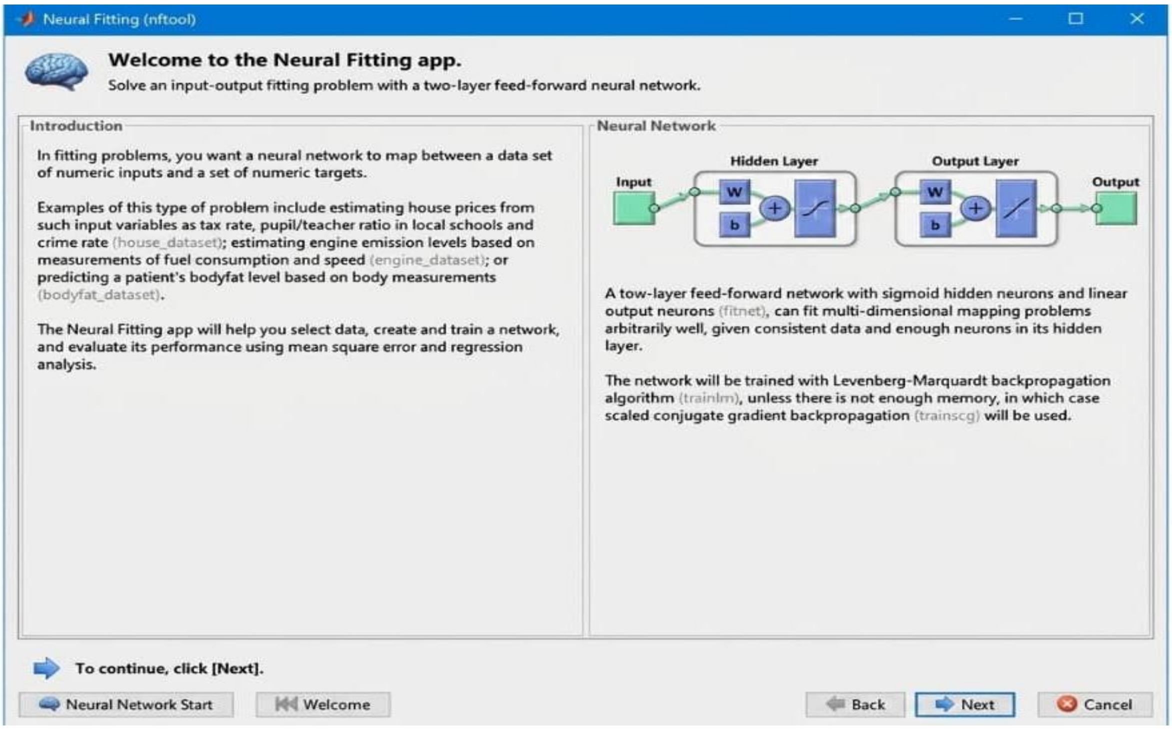

Figure Ⅲ.10. Setting Up the Neural Network Fitting Tool

This figure illustrates the Neural Network Fitting application, highlighting its main objective, which is to address an input-output fitting problem using a two-layer feed-forward neural network.

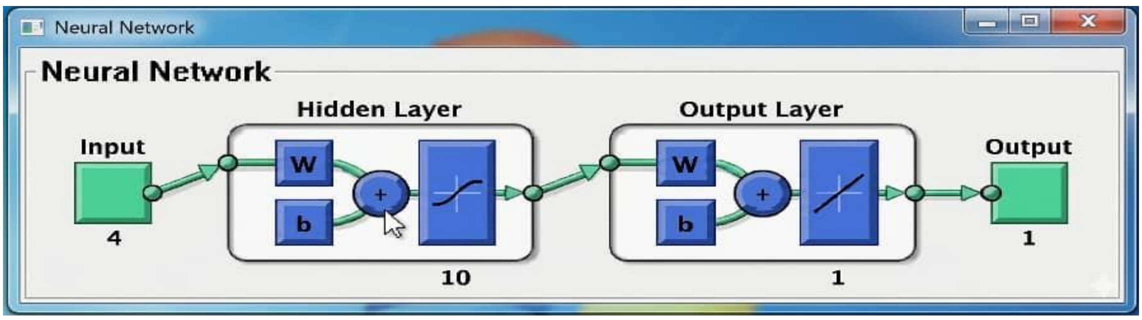

Figure Ⅲ.11. Neural Network Structure

The diagram illustrates the overall structure of the neural network, which consists of an input layer, several hidden layers, and an output layer, where this architecture is used to process data and transform inputs into outputs through the learning process.

Training Algorithm: It is indicated that the neural network will be trained using the Levenberg–Marquardt backpropagation algorithm (trainlm), which is considered an efficient algorithm for improving the speed and accuracy of the training process.

3. Select Data :

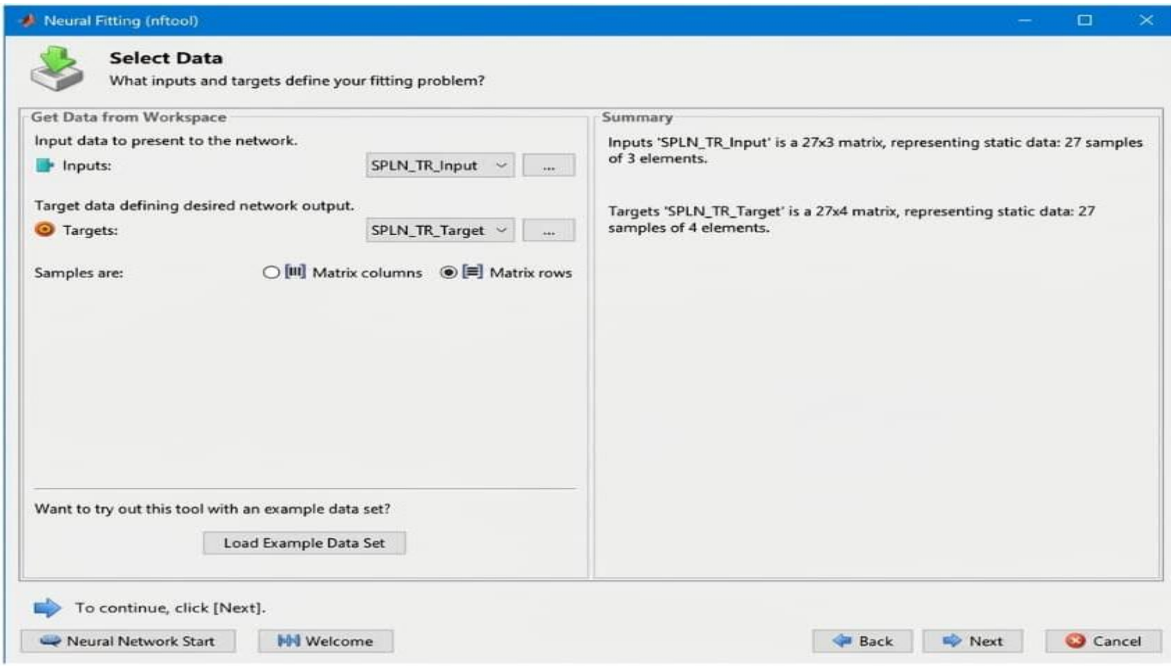

Figure Ⅲ.12. Select Data

Inputs and Targets : This interface allows the selection of input and target data directly from the MATLAB Workspace, facilitating the proper preparation of the dataset used for training the neural network.

Data Summary : The summary displayed on the right shows the dimensions of the selected data. In this example, simplefitInputs and simplefitTargets are used as sample datasets, each containing 94 samples.

4. Import Data :

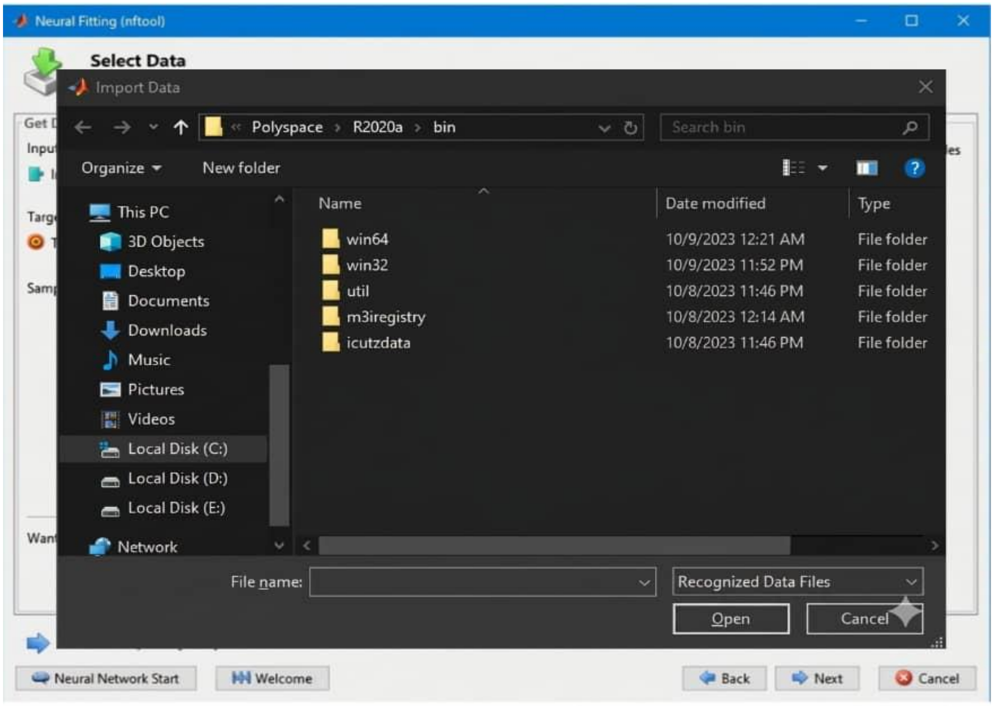

Figure Ⅲ.13. Import Data

<u>Data Import:</u> If the data is not already available in the workspace, this interface allows browsing and importing data files from the computer. This ensures that both input and target datasets are correctly loaded into MATLAB for use in the neural network training process.

5. Validation and Test Data :

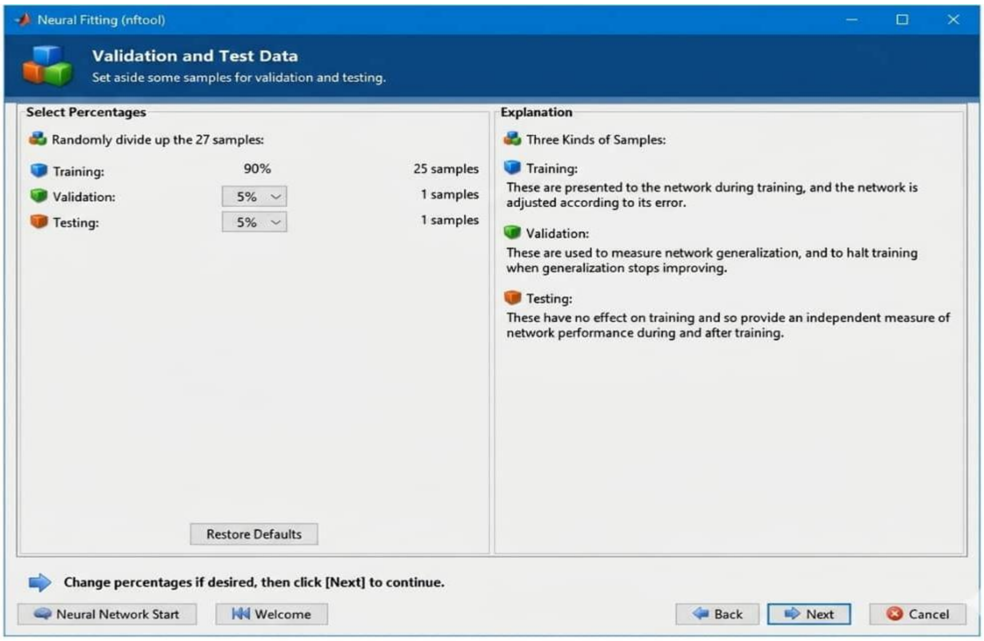

Figure Ⅲ.14. Validation and Test Data

Data Division: This figure illustrates the process of dividing the dataset into three subsets: training, validation, and testing. The default split is 70% for training, 15% for validation, and 15% for testing.

Explanation: Training data is used to train the neural network and adjust its weights, while validation data is used to monitor the model's performance during training and reduce overfitting by stopping the training process when performance degrades. Test data, on the other hand, is used to independently and finally evaluate the network's performance after the training process is completed.

6. Network Architecture :

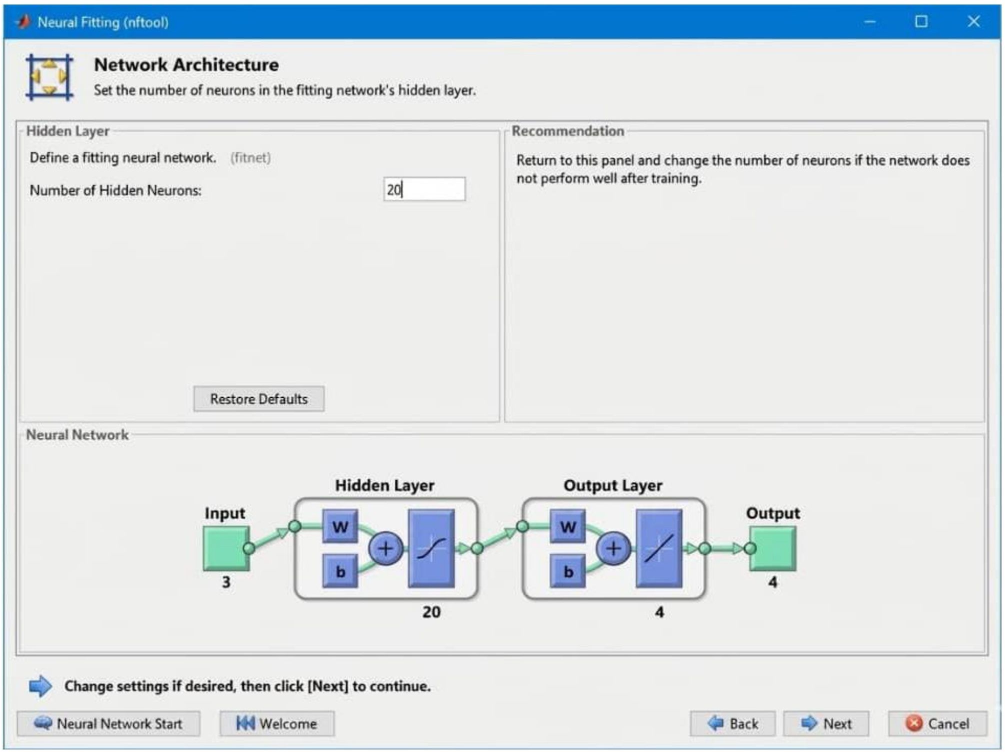

Figure Ⅲ.15. Network Architecture

Hidden Layer Configuration: This interface allows the number of neurons in the hidden layer(s) of the neural network to be defined. In this example, 10 neurons are used in the hidden layer [21].

Network Diagram: The diagram below illustrates a visual representation of the neural network structure, with the number of neurons in the hidden layer defined according to the selected configuration

7. Network Training :

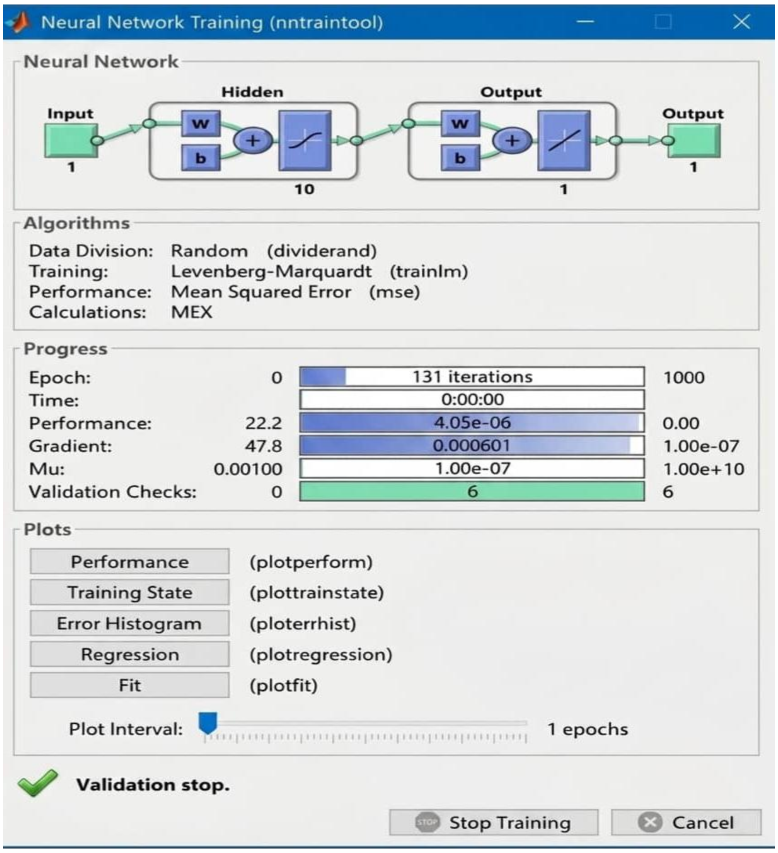

Figure Ⅲ.16. Network Training

Training Process: This figure illustrates the progress of the neural network training process, showing the number of epochs, performance value, gradient, and validation checks, all of which are used to monitor training quality and assess its stability.

Performance Plots: A set of graphical plots is available to monitor the neural network training process and evaluate its performance, including the performance plot, training state plot, error histogram, and regression plots, all of which are used to analyze training quality and model accuracy.

Stop Training: The user can manually stop the neural network training process at any time when necessary [22].

8. Train Network :

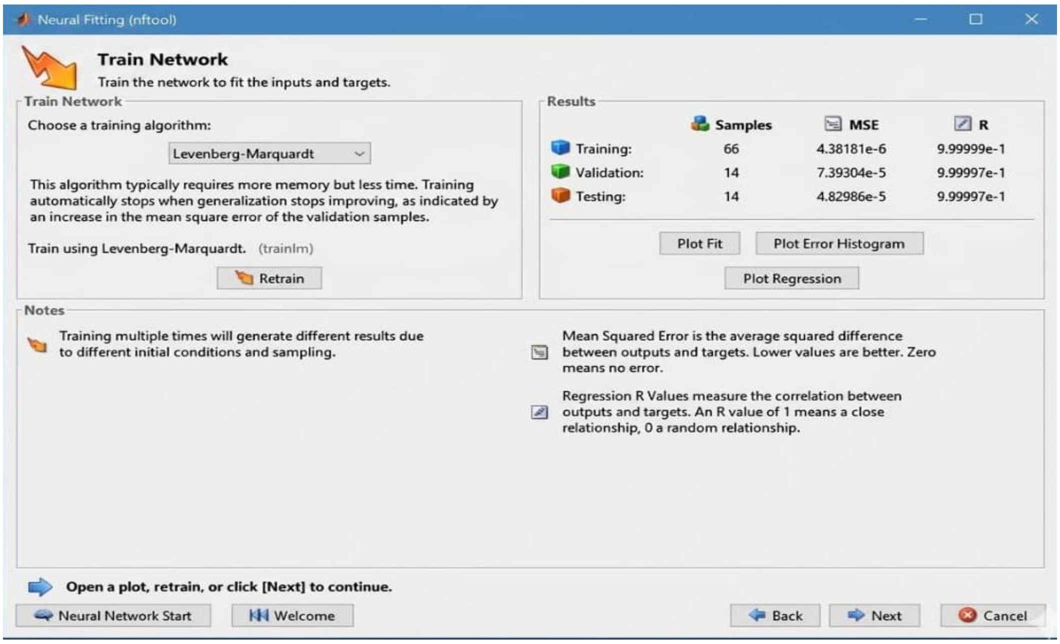

Figure Ⅲ.17. Train Network

<u>Training Results:</u> After completing the training process, this figure presents the final results of the model, including the mean squared error (MSE) values for the training, validation, and testing datasets, which are used to evaluate the accuracy of the neural network's performance

<u>Regression Plot:</u> This plot illustrates the correlation between the neural network outputs and the target values. A correlation coefficient (R) close to 1 indicates a high-quality fit and strong agreement between predicted and actual data.

<u>Error Histogram:</u> This plot illustrates the correlation between the neural network outputs and the target values, where a correlation coefficient (R) close to 1 indicates high accuracy and a good model fit.

The Error Histogram shows the distribution of the differences between the network outputs and the target values, which helps in evaluating the model's accuracy and analyzing the behavior of the errors [22].

III.5.2.5. Fuzzy Logic Control (FLC):

Fuzzy Logic is a form of many-valued logic designed to handle approximate reasoning rather than fixed or binary certainties. Unlike classical logic, which relies on a strict binary dichotomy (True or False), Fuzzy Logic Variables allow for varying degrees of truth. This flexibility enables a Fuzzy Logic Controller (FLC) to achieve high processing speeds and satisfactory accuracy in complex systems.

In such scenarios, a Fuzzy Logic Controller (FLC) can offer both rapid processing speeds and a high level of operational accuracy [23]. The primary objective of the FLC is to monitor and extract the Maximum Power Point (MPP) from a PV system under specific conditions of irradiance (W/m^2) and temperature (℃). A key advantage of this approach is that it does not necessitate comprehensive technical knowledge of the PV system. Furthermore, its inherent simplicity allows it to effectively track the MPP even during periods of fast-varying atmospheric conditions [24]. The FLC has two inputs which are $\frac{dP_{pv}}{dP_{pv}}$ and $\Delta\,(\frac{dP_{pv}}{dP_{pv}})$, (Err) and (ΔErr) which are determined from the PV output power and voltage as follows:

$$E_{rr} = \frac{P_{pv}(K) - P_{pv}(K-1)}{V_{pv}(K) - V_{pv}(K-1)} \quad \textbf{(III.1)}$$

$$\Delta E_{rr} = E_{rr}(K) - E_{rr}(K-1) \quad \textbf{(III.2)}$$

determined from the PV output power and voltage as follows:

The output from the FLC is the required change in the duty cycle of the DC–DC converter (defuzzification). The FLC block diagram is shown in Figure (III.18). The primary advantages of utilizing FLC include its characterization as a universal control algorithm, its simplicity, and its high degree of adaptability. It provides a fast tracking response, maintains parameter insensitivity, and operates effectively even when provided with imprecise input data.

Moreover, the FLC demonstrates superior efficiency in tracking the MPP, particularly during rapidly changing atmospheric conditions [25]. However, a significant limitation arises during PSC, where the controller may become trapped at a LP. Figure (III.19) presents the input and output membership functions, while Table (III.1) outlines the input and output fuzzy rules [26]. The variation step of E_{rr} and E_{rr} may vary according to the system. Once Err and ΔE_{rr} are calculated and transferred to the logic variables based on the membership functions, the FLC output, which is typically duty ratio change, ΔD of the DC–DC boost converter is estimated in rules as given in Table (III.1).

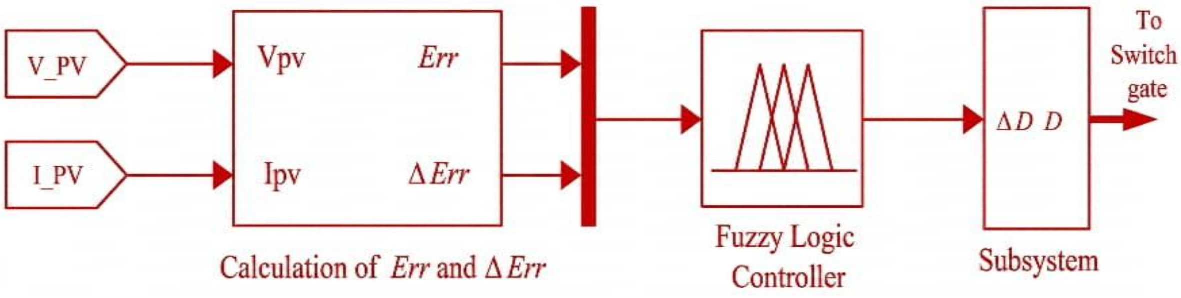

Figure III.18. FLC block diagram in MATLAB/Simulink

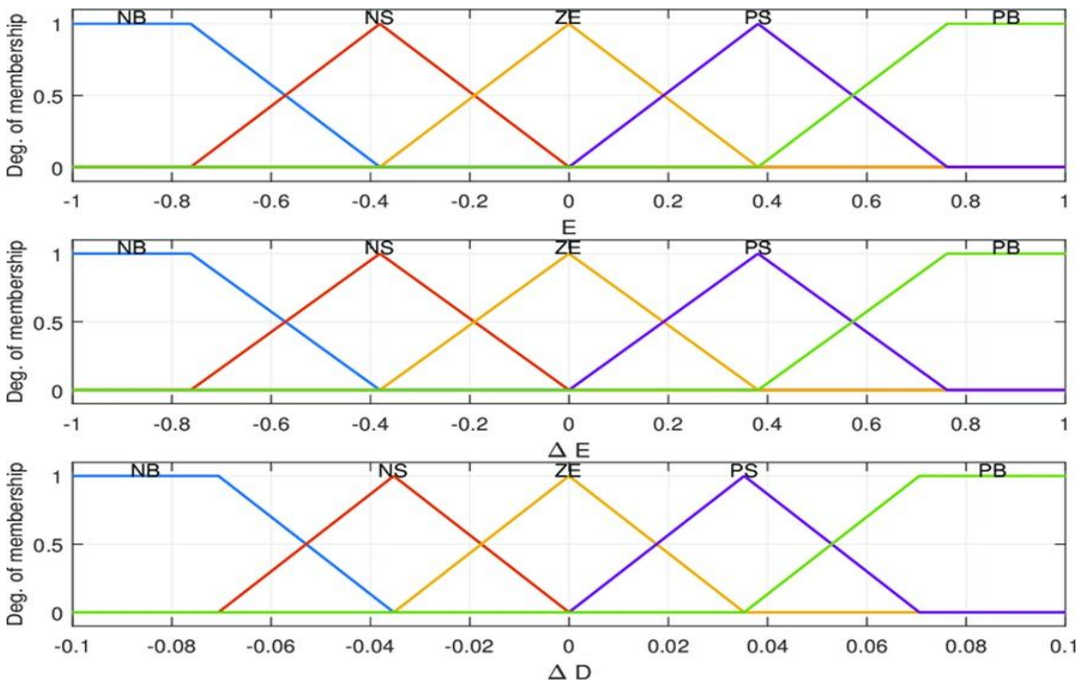

Figure III.19. Membership functions of FLC

Table III.1. Fuzzy rules for the input and output variables

E_{rr}	ΔE_{rr}						
	NB	NM	NS	ZE	PS	PM	PB
NB	NB	NB	NB	NB	NM	NS	ZE
NM	NB	NB	NB	NM	NS	ZE	PS
NS	NB	NB	NM	NS	ZE	PS	PM
ZE	NB	NM	NS	ZE	PS	PM	PB
PS	NM	NS	ZE	PS	PM	PB	PB
PM	NS	ZE	PS	PM	PB	PB	PB
PB	ZE	PS	PM	PB	PB	PB	PB

NB: Negative Big **NM:** Negative Medium **NS:** Negative Small

PB: Positive Big **PM:** Positive Medium **PS:** Positive Small

ZE: Zero

The implementation of this technique for a solar PV system is illustrated in Figure (III.20). During the fuzzification stage, the PV parameters used as inputs are transformed into linguistic variables , whereby crisp quantities are converted into fuzzy quantities (fuzzy sets).

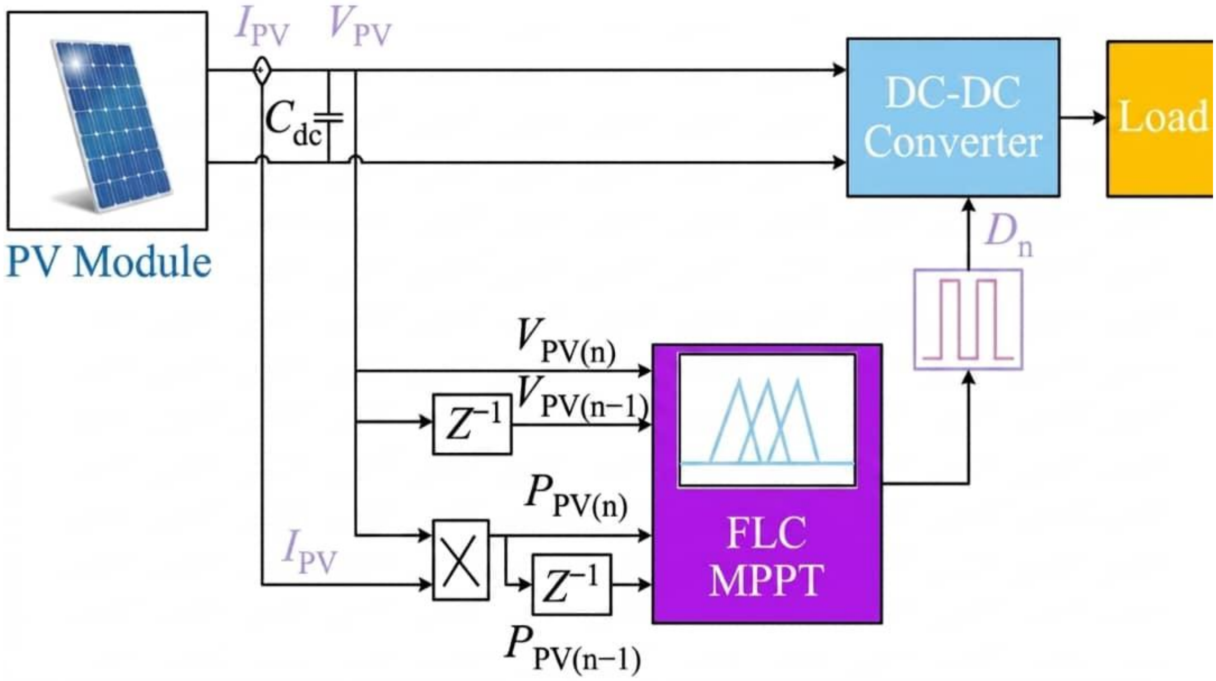

Figure III.20. Block diagram of FLC MPPT technique

Compared to direct and indirect FLC-based MPPT methods, Adaptive FLC demonstrates superior performance during both dynamic and steady-state conditions, irrespective of the converter architecture [27]. In conclusion, to ensure rapid and precise convergence, high tracking efficiency, and the avoidance of drift under PSC, FLC should be integrated with scanning and storing algorithms or other AI techniques to successfully track the GP [28]. The primary advantages and disadvantages of FLC-based MPPT are summarized as follows:

■ Advantages:

- High Robustness and Dynamic Performance: Offers a fast response, superior performance, and adjustable accuracy levels.
- Reduced Oscillation: Minimizes fluctuations during transitions in environmental conditions.
- Tolerance for Imprecision: Capable of operating effectively with imprecise inputs while maintaining high efficiency.
- Synergistic Potential: Becomes significantly more effective when integrated with other EA techniques.

- Model-Free Operation: Does not necessitate an accurate mathematical model or exhaustive technical details of the system.

■ Disadvantages :

- Complexity and Pre-processing: High computational complexity and a potentially costly offline phase, as prior information is mandatory.
- Designer Dependency: The overall efficiency of the system is heavily reliant on the designer's expertise and the precision of the defined fuzzy rules.
- Convergence Issues: May fail to achieve convergence during highly dynamic operating states.
- Static Rule Base: Once the fuzzy rules are defined, they cannot be dynamically altered or updated.

III.6. Conclusion :

In this chapter, the most important and sensitive part of this study has been addressed, where the principle of Maximum Power Point Tracking (MPPT) has been presented along with the various classifications of its control strategies.

The most widely used MPPT methods reported in the literature have also been discussed and analyzed. The existence of multiple approaches demonstrates that this research field is continuously evolving, and that finding one or more universal and unified solutions remains a complex and challenging task.

Chapter IV

Simulation Results

IV.1. Introduction :

In this chapter, we focus on the performance evaluation and comparative analysis of two prominent Maximum Power Point Tracking (MPPT) algorithms: the traditional Perturb and Observe (P&O) and the intelligent Fuzzy Logic Controller (FLC). These algorithms are fundamental to optimizing the power output of photovoltaic (PV) systems by continuously adjusting the operating point to ensure maximum energy extraction under varying environmental conditions.

The P&O algorithm operates on a logic of periodic perturbations and observations to track the optimal point, offering a straightforward implementation. In contrast, the FLC leverages intelligent linguistic rules and an adaptive nature to predict and maintain the maximum power point with significantly higher precision and reduced steady-state oscillations. Our comprehensive analysis aims to highlight the specific performance gaps between these two methods—particularly in terms of tracking speed and stability—to demonstrate why the FLC is often the superior choice for modern, high-efficiency solar energy applications.

IV.2. Parameters of System Simulation :

The following characteristics of panel and the parameters of boost converter that are used in our system simulation, are shown in the figure and table below:

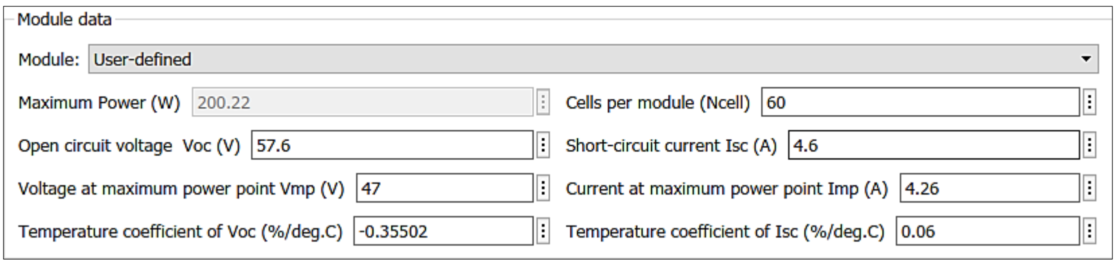
Module data
Module: User-defined
Maximum Power (W) 200.22
Cells per module (Ncell) 60
Open circuit voltage Voc (V) 57.6
Short-circuit current Isc (A) 4.6
Voltage at maximum power point Vmp (V) 47
Current at maximum power point Imp (A) 4.26
Temperature coefficient of Voc (%/deg.C) -0.35502
Temperature coefficient of Isc (%/deg.C) 0.06

Figure Ⅳ.1. Characteristics of Panel

Boost Converter	Value
Capacitor 1	200 µF
Inductor	3.5 mH
Capacitor 2	100 µF
Resistive Load	300 Ω

Table Ⅳ.1. Parameters of Boost Converter

IV.3. Simulation Results :

IV.3.1. P&O Algorithm :

In this simulation, we used the Perturb and Observe (P&O) algorithm to obtain results for power, voltage, and current. Figure (Ⅳ.2) represents the general system simulation, showcasing the overall setup and performance of the P&O -based MPPT system. The figure illustrates the integration of PV panels with the P&O -based MPPT controller, which adjusts the duty cycle to optimize power extraction.

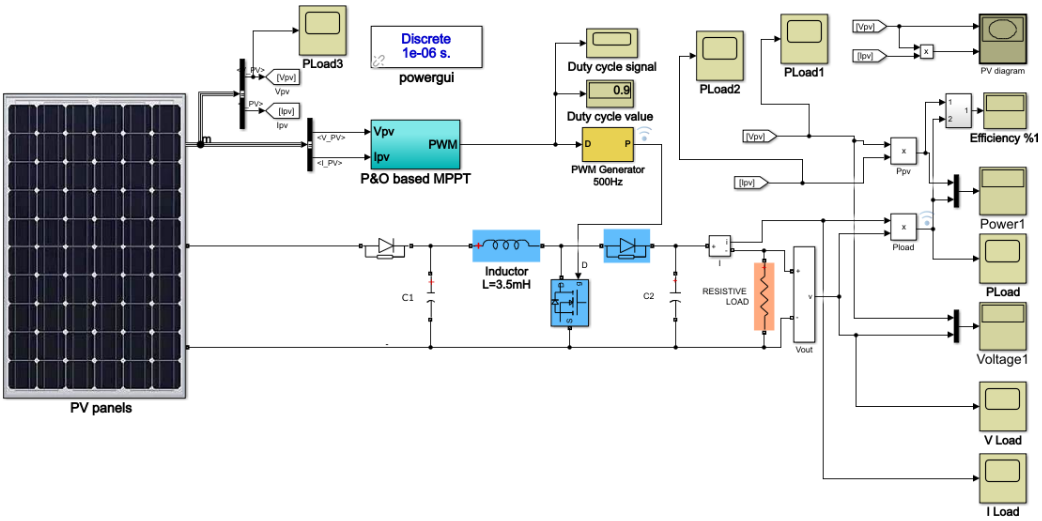

Figure Ⅳ.2. Schema of System Simulation With P&O

a).Constant Irradiance (1000 W/m2) :

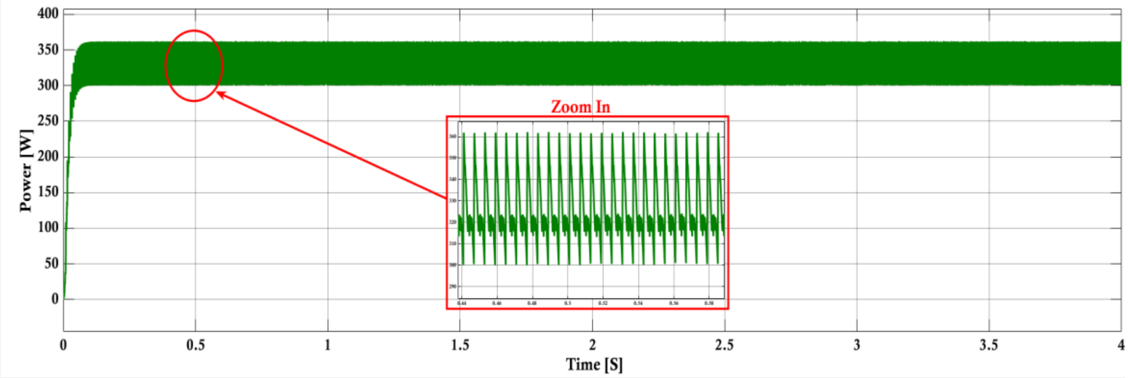

Figure Ⅳ.3. Power Simulation Result

The Figure (Ⅳ.3) illustrates the power response of an MPPT system using the P&O algorithm. The main plot shows a rapid increase in power followed by stabilization around 350W. The zoomed-in view highlights the oscillatory nature of the power output, characteristic of the P&O algorithm as it continuously perturbs to track the maximum power point. These oscillations are a trade-off for maintaining optimal power extraction and are crucial for understanding the efficiency and performance of the MPPT system.

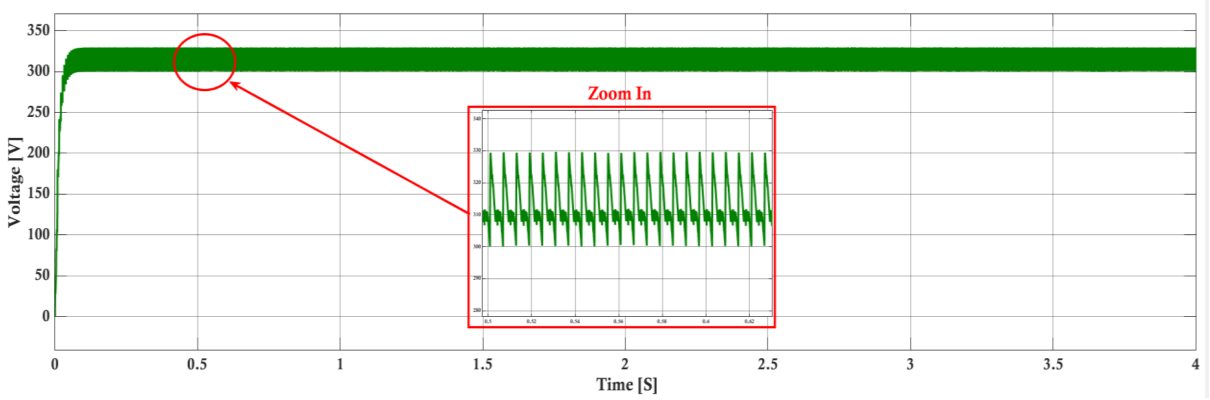

Figure Ⅳ.4. Voltage Simulation Result

The Figure (Ⅳ.4) illustrates the voltage response of an MPPT system using the P&O algorithm. The main plot shows a rapid increase in voltage, stabilizing around 320V. The zoomed-in view highlights the oscillatory nature of the voltage output.

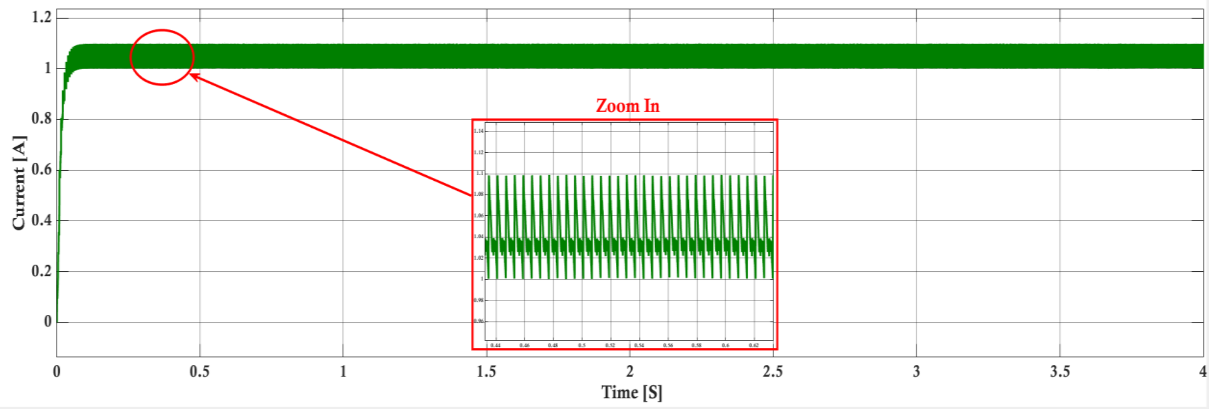

Figure Ⅳ.5. Current Simulation Result

The Figure (Ⅳ.5) illustrates the current response of an MPPT system using the P&O algorithm. the main plot shows the rapid transient response leading to stabilization at approximately 1.05A, indicative of the system reaching its maximum power point. The zoomed-in view provides a closer look at the inherent oscillations around this steady-state value.

b).Variable Irradiances (1000, 800, 600, 400 W/m^2) :

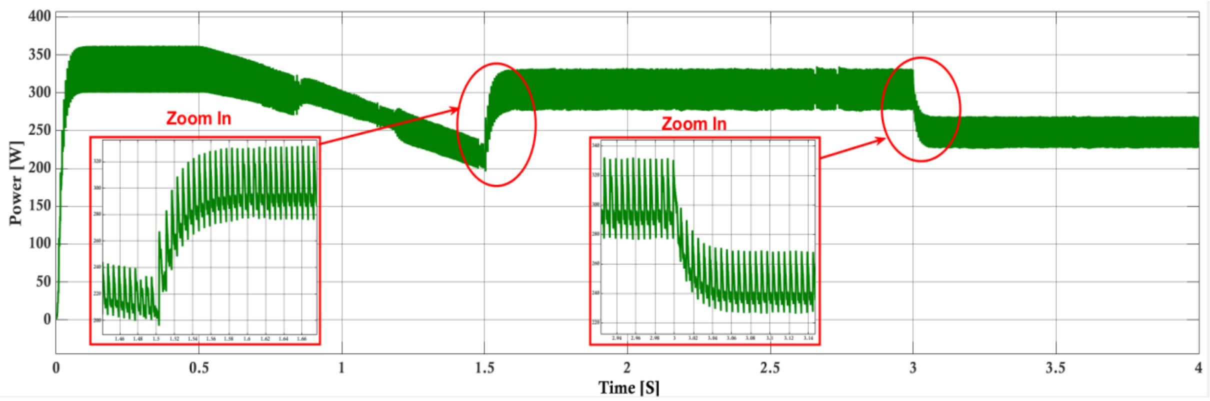

Figure Ⅳ.6. Power Simulation Result

The Figure (Ⅳ.6) provides a comprehensive view of the MPPT system's power output behaviour under varying irradiance levels. The main plot demonstrates the system's ability to track the maximum power point (MPP) across different irradiances, with the power stabilizing at the following approximate levels:

- 360 W (Initial peak/plateau)
- 330 W (Between 1.5s and 3s)
- 260 W (After the drop at 3s)

The red ellipses and zoomed-in views emphasize the system's transient response to sudden changes in irradiance-specifically at t = 1.5s (an increase) and t = 3s (a decrease). These views showcase the characteristic oscillations and the settling time as the P&O algorithm adjusts to the new maximum power point. This detailed analysis underscores the efficiency and adaptability of the MPPT system in real-time solar energy applications.

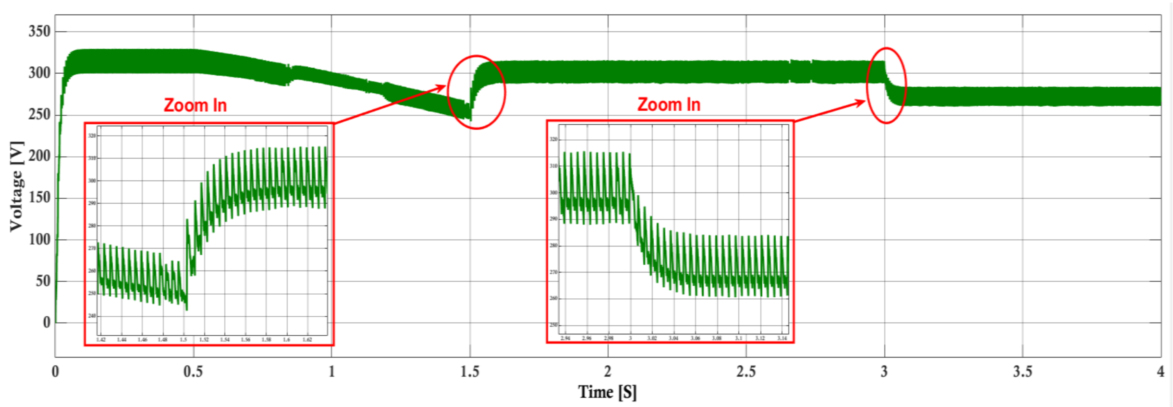

Figure Ⅳ.7. Voltage Simulation Result

The Figure (Ⅳ.7) demonstrates how the voltage of an MPPT system using the P&O algorithm adjusts to varying irradiance levels over a 4-second period.

- The main plot shows the system's quick voltage stabilization at approximately 325 V initially.
- Following the fluctuations between 0.5s and 1.5s, the voltage stabilizes again at roughly 315 V.
- at t = 3s, the system exhibits a stepwise decrease, settling at a new level of approximately 275 V as the irradiance drops.

The red circled zoomed-in views provide a detailed look at the transient fluctuations at the 1.5s and 3s marks. These illustrate the algorithm's continuous oscillations and rapid adjustments to maintain optimal performance despite the changing environmental conditions.

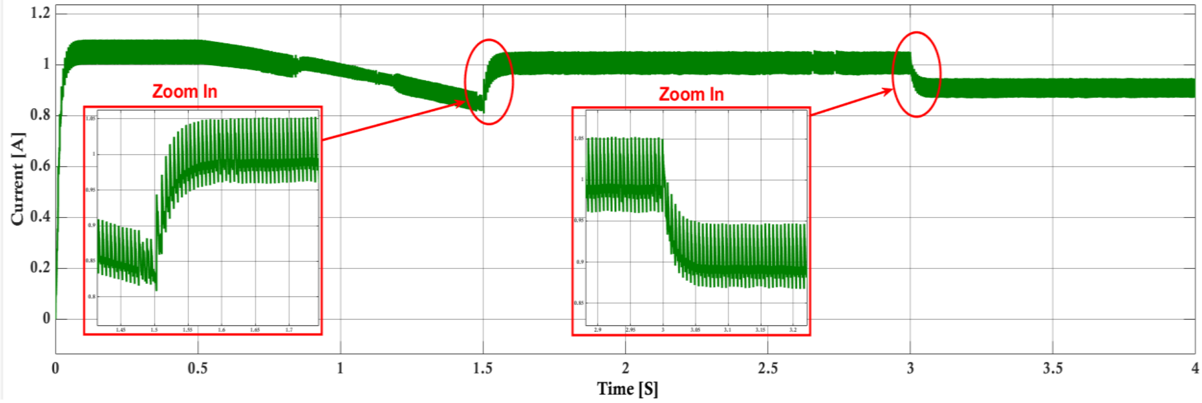

Figure Ⅳ.8. Current Simulation Result

The Figure (Ⅳ.8) demonstrates how the MPPT system's current output, managed by the P&O algorithm, adjusts under varying irradiance levels over time. The main plot shows the current initially stabilizing around 1.05 A. Following the fluctuations, it stabilizes again at approximately 1.0 A between 1.5s and 3s. At t = 3s, the current decreases in a stepwise manner, settling at a new level of approximately 0.9 A as the irradiance diminishes. The zoomed-in views capture the detailed transient response and the characteristic oscillations during these irradiance changes at 1.5s and 3s.

IV.3.2. Fuzzy Logic Controller (FLC) algorithm:

In this simulation, we used the Fuzzy Logic Controller (FLC) algorithm to obtain results for power, voltage, and current. Figure (IV.9) represents the general system simulation, showcasing the overall setup and performance of the FLC-based MPPT system. The figure illustrates the integration of PV panels with the FLC-based MPPT controller, which adjusts the duty cycle to optimize power extraction.

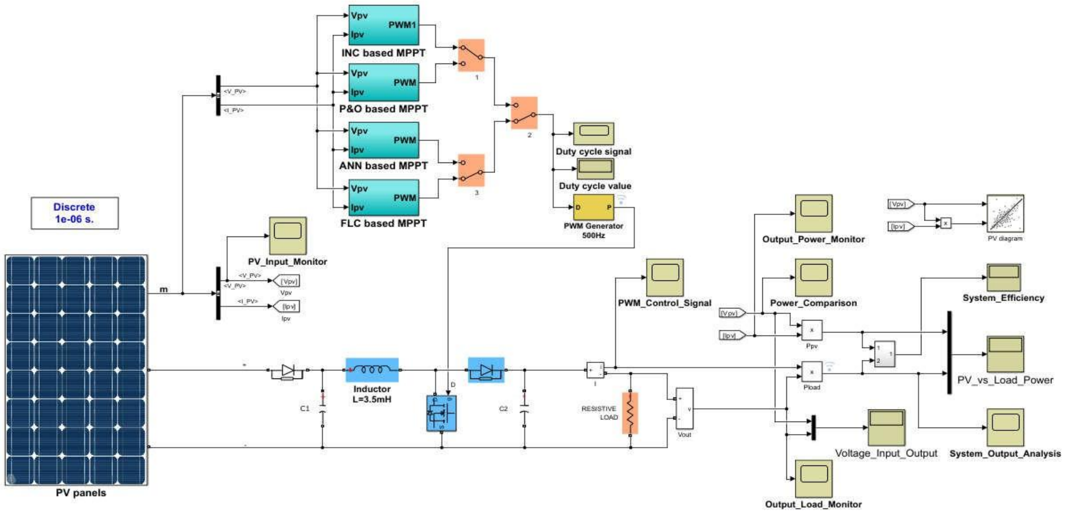

Figure IV.9. Schematic simulation system with FLC

a)- Constant irradiance (1000 W/m²) and constant temperature (25°C):

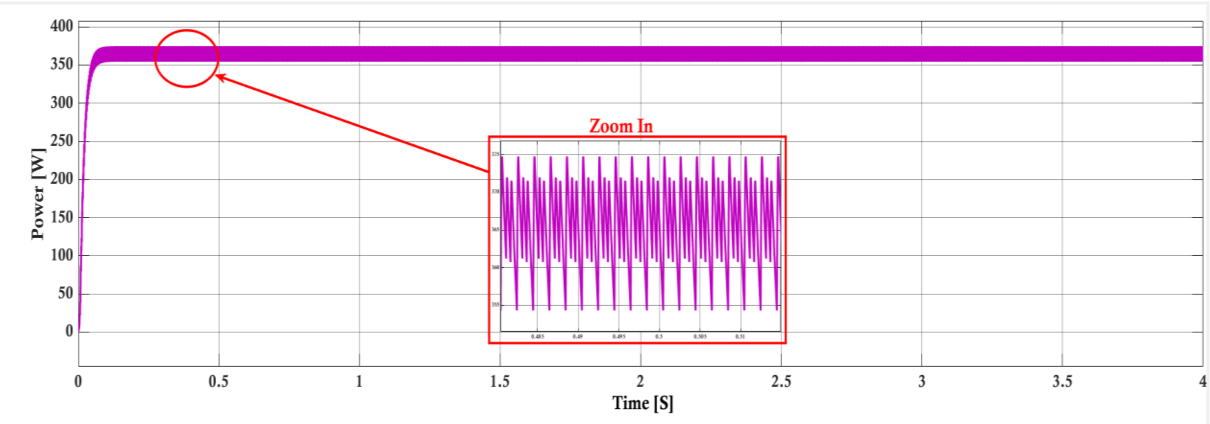

Figure IV.10. Power simulation result versus time for FLC in constant irradiance

The figure (IV.10) illustrates the system power output exponentially increasing quickly to around 370 W under constant irradiance, controlled by a Fuzzy Logic Controller (FLC). After this initial rise (transient time), the power stays fairly stable around this value but shows continuous, relatively small-scale, cyclical fluctuations (steady-state). Zooming in stresses these oscillations, suggesting natural dynamics or control reactions within the FLC-controlled system. The FLC performs well in regulating the average power, but there is a steady-state ripple.

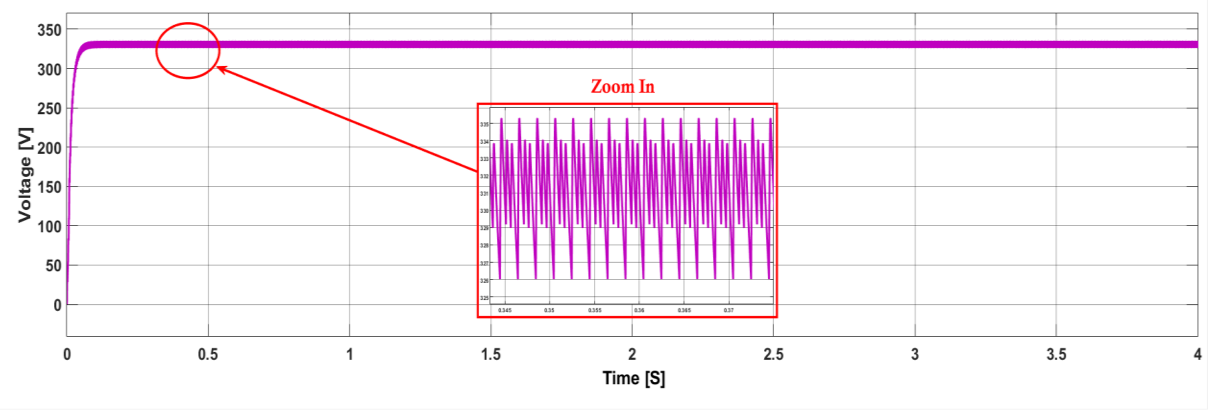

Figure IV.11. Voltage simulation result versus time for FLC in constant irradiance

The figure represents the voltage behaviour of an FLC-based MPPT system under constant irradiance conditions. The curve shows a rapid rise in voltage, quickly stabilizing around a specific value (approximately 335V). This indicates the system's ability to adapt efficiently and reach optimal performance under stable environmental conditions. While the zoomed-in views the magnified section reveals minor fluctuations after stabilization, reflecting the system's continuous fine-tuning to maintain maximum power point tracking with high precision despite minor load or condition changes.

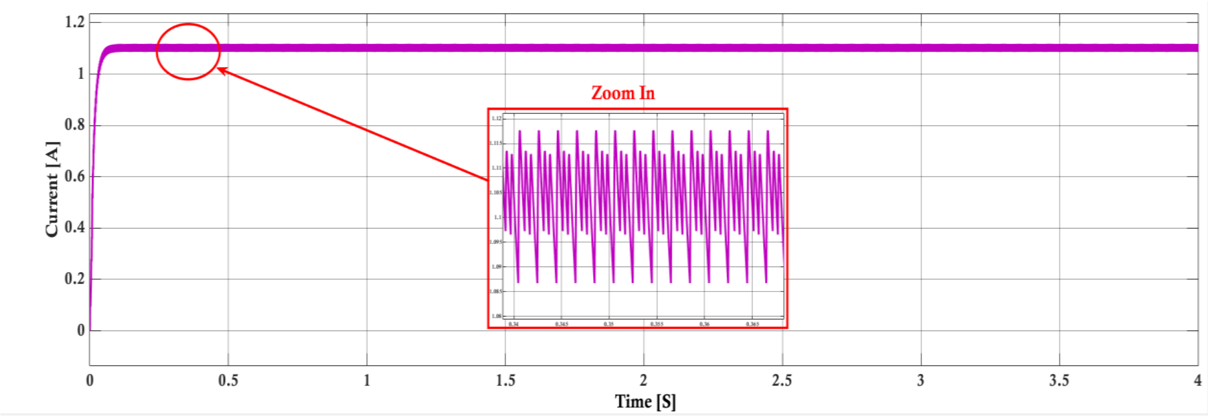

Figure IV.12. Current simulation result versus time for FLC in constant irradiance

The Figure (IV.12) illustrates the current stabilization of an FLC-based MPPT system. The main plot shows a rapid rise in current, stabilizing around 1.1A. The zoomed-in view highlights small fluctuations near the stabilization point. This behaviour reflects the efficiency of the FLC system under constant irradiance conditions, with minor deviations due to its rule-based nature.

b)- Variable irradiances (1000, 800, 600, 400 W/m²) and constant temperature (25°C):

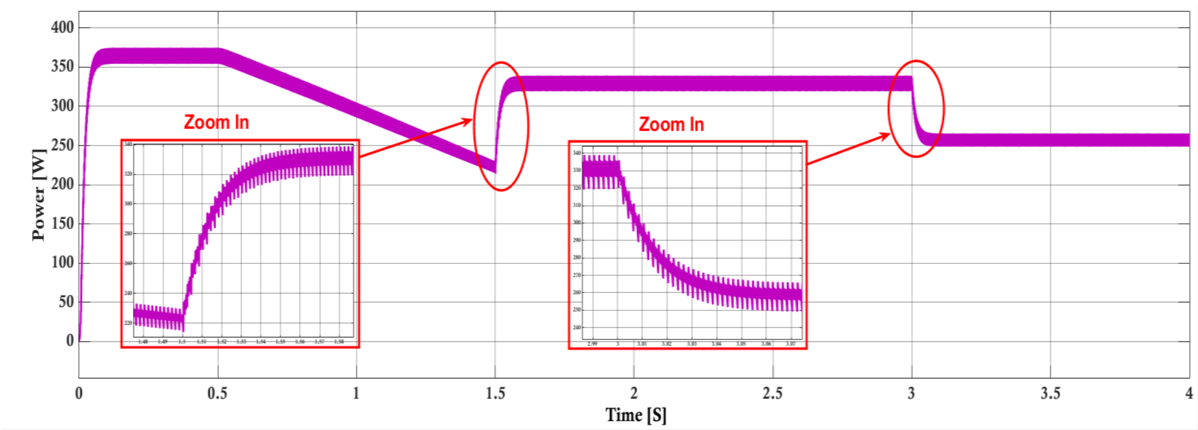

Figure IV.13. Power simulation result versus time for FLC in variable irradiances

The figure illustrates the performance of the Fuzzy Logic Controller (FLC) based MPPT system under fluctuating irradiance conditions.

- Initially, the power stabilizes at approximately 365 W.
- Following changes in irradiance, the system tracks new levels, stabilizing at roughly 330 W between 1.5s and 3s.
- After a final drop at t = 3s, the power settles at approximately 260 W.

The zoomed-in sections highlight the transient behaviour during these transitions. For instance, in the second zoom-in at t = 3s, the power is shown dropping from a range of 320 W – 340 W down to the 260 W level. These precise adjustments demonstrate the system's ability to dynamically adapt to rapid changes in irradiance while maintaining efficient energy extraction with the reduced oscillations typical of an FLC.

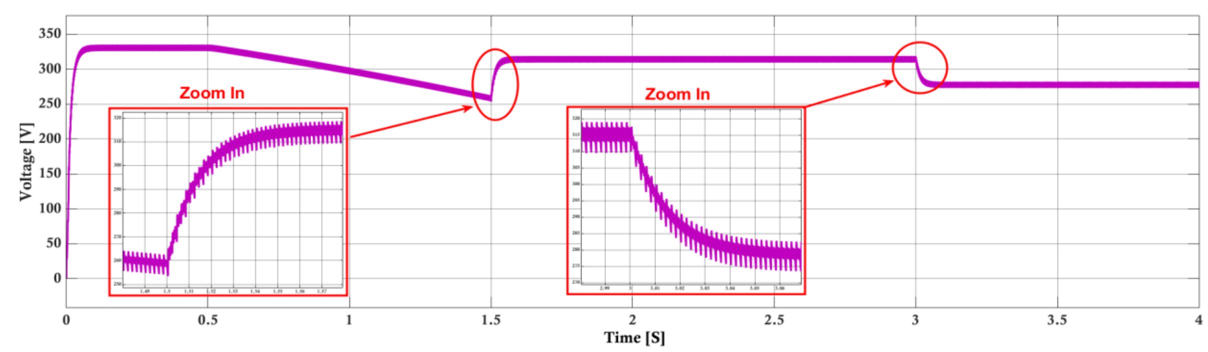

Figure IV.14. Voltage simulation result versus time for FLC in variable irradiances

The Figure (IV.14) illustrates the FLC-based MPPT system's voltage response to varying irradiance conditions.

- The main plot shows the system's initial voltage stabilization at approximately 330 V.
- Between 1.5s and 3s, the voltage maintains a steady plateau at roughly 315 V.

- Following the irradiance change at t = 3s, the voltage steps down to settle at approximately 278 V.

The zoomed-in views reveal the transient fluctuations during adaptation. Specifically, the first zoom-in highlights a transition from roughly 260 V up to 315 V starting at 1.5s. Each stabilization period after these irradiance changes is highly efficient, taking approximately 0.05 to 0.08 seconds to reach a steady state. This performance demonstrates the FLC algorithm's ability to quickly adapt to dynamic solar irradiance changes while maintaining stable performance with minimal ripple.

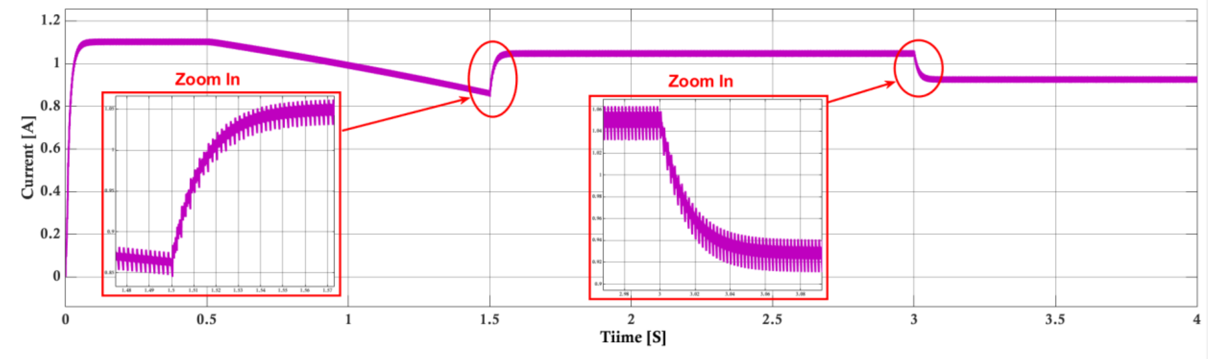

Figure IV.15. Current simulation result versus time for FLC in variable irradiances

The Figure (IV.15) depicts the current response of an FLC-based MPPT system under fluctuating irradiance levels. Initially, the current stabilizes at approximately 1.1 A, showing steady behaviour. Between 1.5s and 3s, the current maintains a stable level at approximately 1.05 A. As the irradiance drops at t = 3s, the current exhibits a stepwise reduction, settling at roughly 0.92 A. The zoomed-in sections highlight the transient behaviour during these transitions. The first zoom-in captures the recovery from approximately 0.85 A back to the 1.05 A plateau starting at 1.5s. These views reflect the system's dynamic adaptation to rapid changes in irradiance, with the FLC effectively minimizing oscillations to maintain a smooth output throughout the simulation.

IV.5. Comparison and Analysis Between (P&O, FLC):

IV.5.1. Constant Irradiance (1000 W/m^2) :

The following figures compare the current and voltage outputs of three MPPT algorithms: Perturb and Observe (P&O), and Fuzzy Logic Controller (FLC).

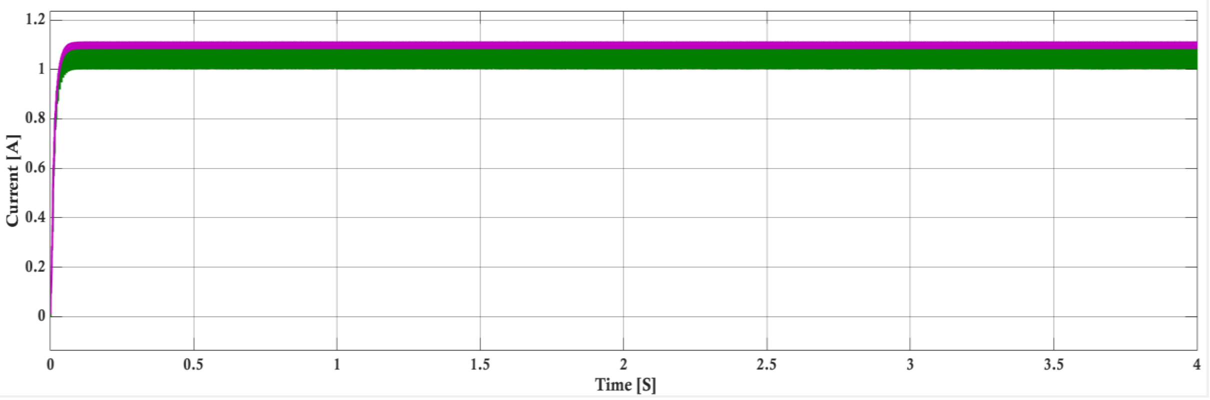

Figure Ⅳ.16. Current Simulation Result

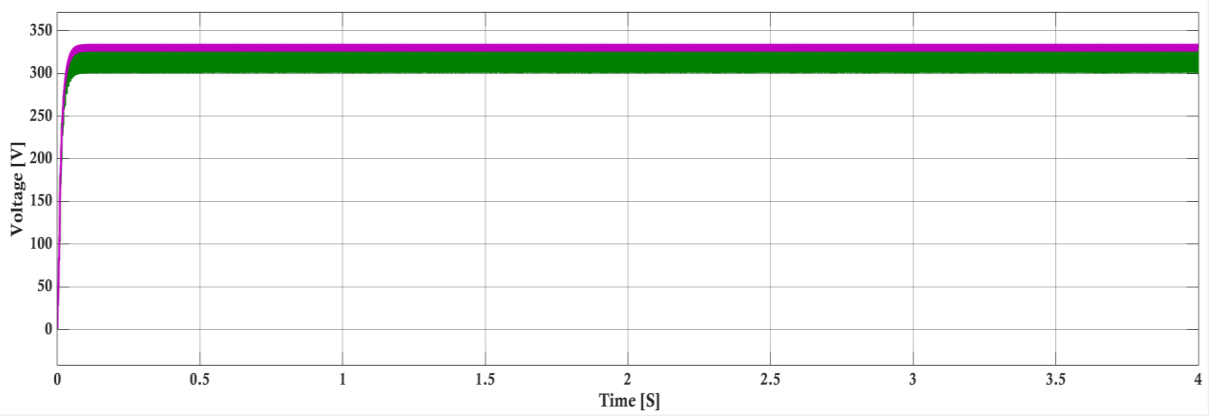

Figure Ⅳ.17. Voltage Simulation Result

(1) Comparison:

• Fuzzy Logic Control (FLC) — Purple Trace: This algorithm demonstrates superior performance with rapid stabilization in both current and voltage. As shown in the plots, it stabilizes at approximately 1.1 A and 330 V, exhibiting minimal fluctuations around the Maximum Power Point (MPP). This indicates high efficiency and a very stable response with nearly zero steady-state ripple.

• Perturb and Observe (P&O) — Green Trace: While this algorithm is capable of reaching a stabilization point quickly, it stabilizes at slightly lower average values of roughly 1.05 A and 315 V. It suffers from significant continuous oscillations (fluctuations) in both current and voltage throughout the simulation. These steady-state oscillations represent a constant loss of energy and lower overall stability compared to the FLC approach.

(2) Analysis:

- Superiority of FLC (Purple): Based on the simulation results, the Fuzzy Logic Controller (FLC) significantly outperforms the traditional P&O method. The primary advantage visible in the graphs is its ability to eliminate the heavy oscillations inherent in the P&O approach. By utilizing linguistic rules, the FLC provides a much smoother response and more precise tracking, stabilizing at higher values of approximately 1.1 A and 330 V. This precise stabilization maximizes the overall power output of the PV system.

- Efficiency Gap: While the P&O (Green) algorithm is simpler to implement, its "blind" step-by-step searching leads to continuous instability once the peak is reached. This is clearly evidenced by the thick green bands in the images, indicating persistent fluctuations. In contrast, the FLC's adaptive nature allows it to settle accurately at the peak with negligible ripple, making it the more efficient and reliable option for optimizing photovoltaic performance.

The Fuzzy Logic Control (FLC) algorithm is the optimal choice for this MPPT system, offering superior stability, higher extraction efficiency, and significantly reduced fluctuations compared to the traditional P&O algorithm.

IV.5.2. Variable Irradiances (1000, 900, 800, 700, 600 W/m^2) :

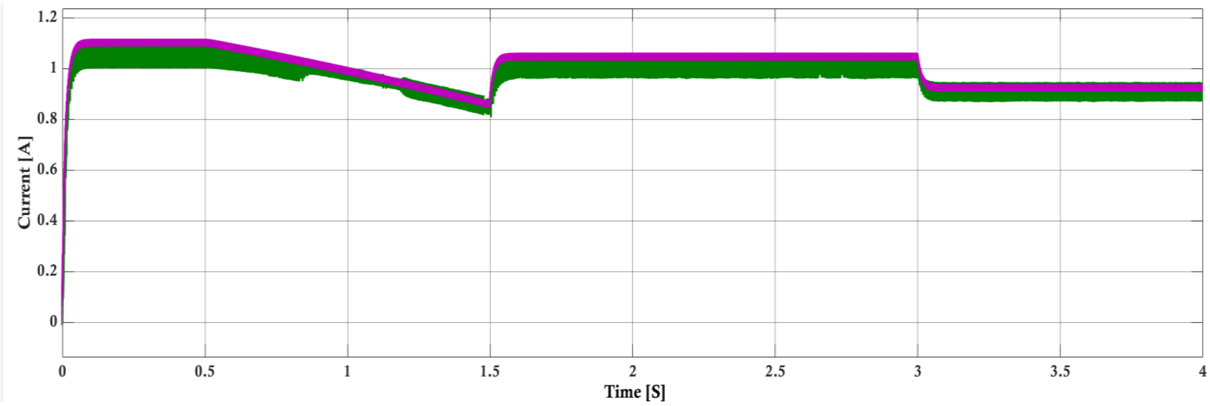

Figure Ⅳ.18. Current Simulation Result

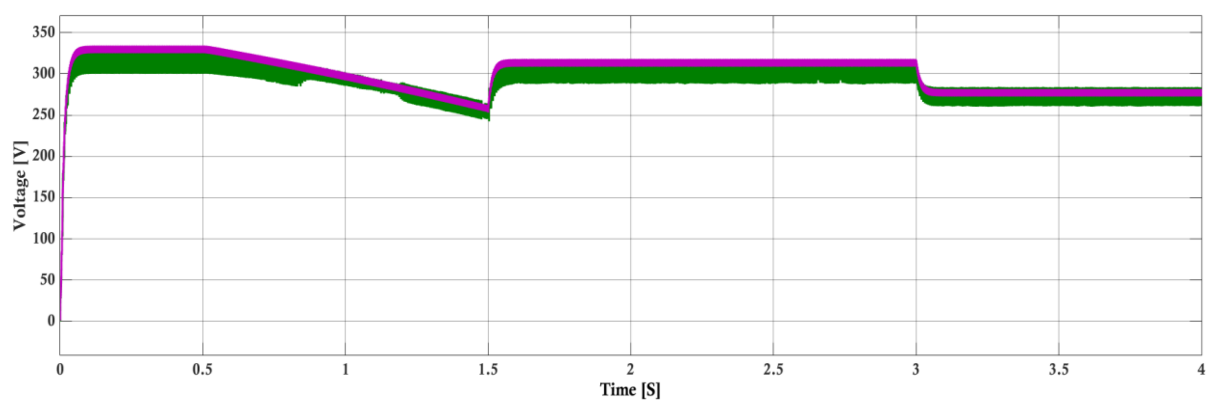

Figure Ⅳ.19. Voltage Simulation Result

(1).Comparison:

- Fuzzy Logic Control (FLC) — Purple Trace: This algorithm exhibits the least fluctuations and the smoothest transitions during rapid changes in irradiance, such as the transitions at t = 1.5s and t = 3s. It stabilizes quickly at higher values—approximately 1.1 A and 330 V initially—and maintains a steady output at the maximum power point with negligible ripple, indicating high stability and superior extraction efficiency.
- Perturb and Observe (P&O) — Green Trace: This algorithm shows noticeable and continuous oscillations around the maximum power point throughout the simulation. It is significantly less stable during transitions between irradiance levels, leading to energy losses in both transient and steady states, settling at lower average levels of approximately 1.05 A and 315 V.

2) Analysis:

- Best Performance: The Fuzzy Logic Control (FLC) algorithm demonstrates the best performance. Unlike P&O, which struggles with the trade-off between tracking speed and oscillation (visible in the thick green bands), FLC uses intelligent linguistic rules to achieve high precision with minimal deviations.
- Technological Edge: The FLC algorithm has a significant edge over the Perturb and Observe (P&O) algorithm due to its adaptive nature. It handles the non-linear characteristics of the PV system more effectively under dynamic weather conditions, whereas P&O exhibits persistent instability and higher ripple when irradiance changes.

Based on these figures, the Fuzzy Logic Control (FLC) algorithm is the optimal choice for MPPT, offering the most stable and efficient performance under varying irradiance conditions.

IV.6. Comparison of efficiency between algorithms (P&O, FLC):

IV.6.2. Variable Irradiances (1000, 800, 600, 400 W/m^2) :

Algorithm	**Efficiency**
Perturb and Observe (P&O)	91.89%
Fuzzy Logic Controller (FLC)	92.71%

Table Ⅳ.2. Table of Efficiency

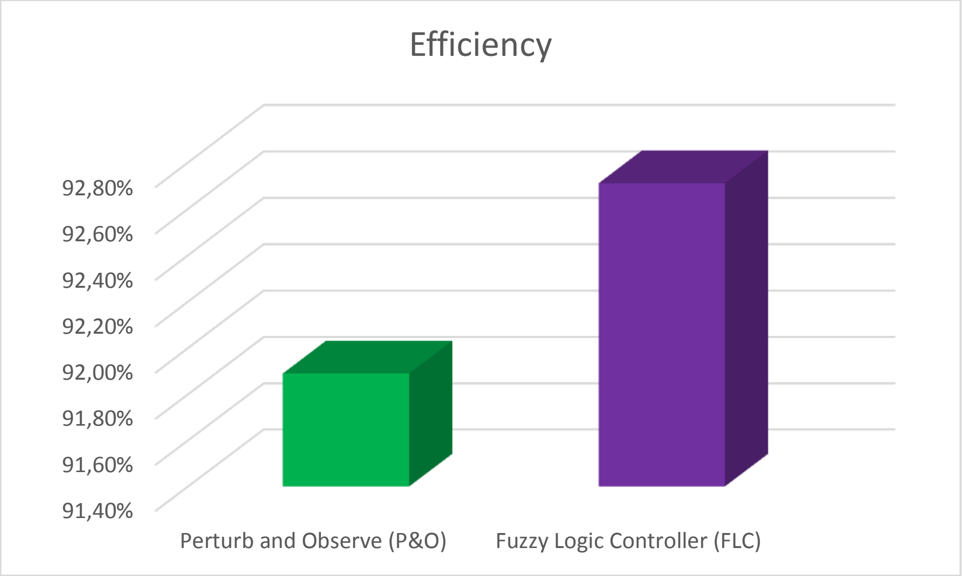

Figure IV.21. Chart of Efficiency

Under variable irradiance conditions, the Fuzzy Logic Control (FLC) algorithm demonstrates the highest efficiency, around 92.71%, indicating its superior ability to adapt rapidly to changing light conditions. In contrast, the Perturb and Observe (P&O) algorithm reaches an efficiency of approximately 91.89%, reflecting its greater susceptibility to heavy fluctuations and its tendency to lose track of the maximum power point during sudden irradiance shifts. These results highlight the FLC algorithm's effectiveness in optimizing power output in dynamic environments, as its intelligent rule-base allows it to respond to transients much more accurately than the conventional P&O method.

IV.6.1. Constant Irradiance (1000 W/m^2) :

Algorithm	Efficiency
Perturb and Observe (P&O)	93.18%
Fuzzy Logic Controller (FLC)	94.55%

Table IV.1. Table of Efficiency

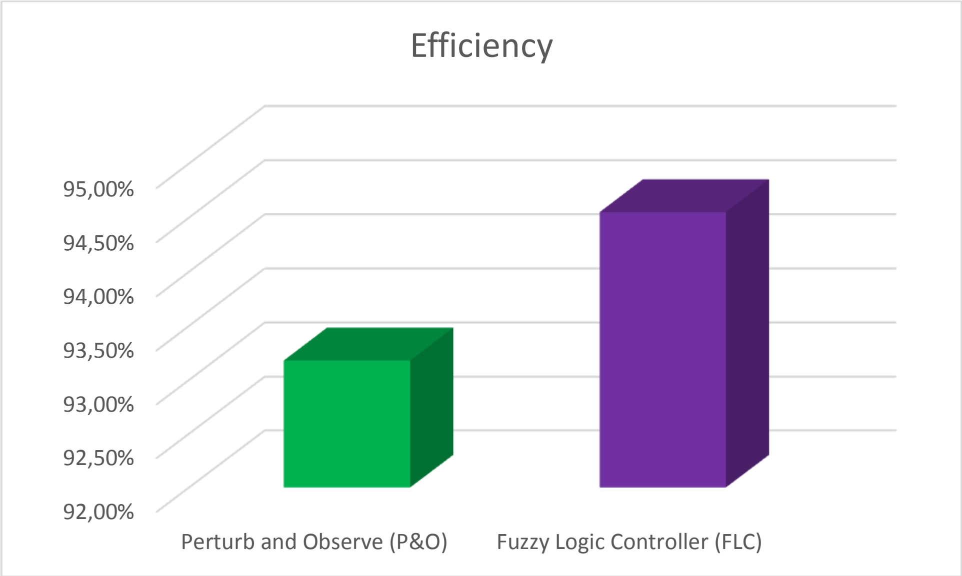

Figure IV.20. Chart of Efficiency

Under a constant irradiance of 1000 W/m², the Fuzzy Logic Control (FLC) algorithm demonstrates the highest efficiency, reaching approximately 94.55%. In contrast, the Perturb and Observe (P&O) algorithm exhibits a lower efficiency of approximately 93.18%. This gap is primarily due to the P&O algorithm's inherent oscillations around the maximum power point, which result in continuous power losses. These results indicate that the FLC algorithm is more effective in optimizing power output under stable irradiance conditions, significantly outperforming the traditional P&O method in both precision and energy harvesting.

IV.7. Conclusion :

The Fuzzy Logic Control (FLC) algorithm stands out as the most effective and reliable MPPT method in this study. Its superior efficiency, stability, and adaptability under both steady and dynamic irradiance conditions make it the best choice for optimizing photovoltaic system output. Despite its common use in basic applications, the Perturb and Observe (P&O) algorithm proved to be the least effective in this comparison, demonstrating lower efficiency and greater instability due to continuous oscillations. Therefore, for maximizing energy extraction and ensuring reliable performance under varying climatic conditions, the FLC algorithm is the recommended MPPT method for this PV system.

General Conclusion

General Conclusion

This study began by laying the foundation for understanding solar radiation and photovoltaic energy conversion principles. It explained how solar cells harness the photovoltaic effect to generate electricity from sunlight and discussed the modeling, characteristics, and factors influencing the efficiency of photovoltaic generators. Different photovoltaic cell types based on silicon crystal structures were also presented.

Building upon this, the crucial role of DC-DC converters in power management systems was explored. These converters facilitate efficient voltage conversion through various topologies like buck, boost, and buck-boost, enabling their widespread use across diverse industries.

The concept of Maximum Power Point Tracking (MPPT) was then introduced as a vital technology, particularly for renewable energy systems. MPPT algorithms optimize energy extraction by continually adjusting the electrical operating point to track the maximum power output of photovoltaic panels.

This naturally led to an in-depth examination of MPPT principles, classifications, and implementation methods. Among the algorithms evaluated, the Fuzzy Logic Control (FLC) approach emerged as the most effective and reliable. Its superior efficiency, stability, and adaptability under both steady and dynamic irradiance conditions make it the recommended method for maximizing energy extraction and ensuring robust performance in photovoltaic systems.

While the commonly used Perturb and Observe (P&O) method is simple to implement, it fell short of the advanced capabilities offered by FLC-based MPPT, particularly due to its inherent oscillations and slower response to atmospheric changes. Consequently, for optimizing photovoltaic system output and ensuring long-term, reliable operation, the FLC algorithm stands out as the optimal solution among the methods studied.

References

[1] B. Nour-Eddine, "Amélioration des performances de contrôle d’un système photovoltaïque par les méthodes métaheuristques," El Oued, Université Echahid Hamma Lakhdar. Faculté des Sciences et Technologie, 2013.

[2] S. Y. BOUDERHEM BRAHIM "Conception et Réalisation d’un Hacheur Boost MPPT à Base d’une Carte ARDUINO Application PV," 2017.

[3] S. Dwari and L. Parsa, "An efficient high-step-up interleaved DC–DC converter with a common active clamp," *IEEE Transactions on Power Electronics*, vol. 26, no. 1, pp. 66-78, 2010.

[4] F. L. Luo and H. Ye, *Advanced dc/dc converters*. crc Press, 2016.

[5] A. S. Y. Alzahrani, *Advanced topologies of high-voltage-gain DC-DC boost converters for renewable energy applications*. Missouri University of Science and Technology, 2018.

[6] R. P. Severns, G. Bloom, and R. P. Severns, *Modern DC-to-DC switchmode power converter circuits*. Springer, 1985.

[7] S. Chakraborty, H.-N. Vu, M. M. Hasan, D.-D. Tran, M. E. Baghdadi, and O. Hegazy, "DC-DC converter topologies for electric vehicles, plug-in hybrid electric vehicles and fast charging stations: State of the art and future trends," *Energies*, vol. 12, no. 8, p. 1569, 2019.

[8] https://www.toolify.ai/ai-news/complete-tutorial-implementing-ann-in-matlabsimulink-1764419#google_vignette (accessed.

[9] M. D. S. M. C. Mr MEKKAOUI Saddam and AhmedYahia, "(Conception, simulation et réalisation d’un régulateur solaire avec commande MPPT à base d’une carte Arduino) ", UNIVERSITE EchahidHamma Lakhdar- EL Oued, 2022.

[10] M. K. B. Abdelheq, "ETUDE ET REALISATION D’UN CONVERTISSEUR DC-DC," Université Aboubakr BelkaÔd-Tlemcen, 2018.

[11] S. ABBOUDA, "« Contribution à la commande des systèmes photovoltaïques »," Université de Reims Champagne-Ardenne et université de Sfax, 2015.

[12] R. Touahir and M. B. Zahia, "contrôleur neuronal pour la poursuite du point de puissance maximale d'un système photovoltaïque," *Mémoire master, Université Kasdi Merbah, Ouargla, Algérie,* 2015.

[13] S. H. E. Babaa, "High efficient interleaved boost converter with novel switch adaptive control in photovoltaic application," Newcastle University, 2013.

[14] A. b. T. Bekhti Mohammed, "Maximum Power Point Tracking Simulations for PV Applications Using Matlab Simulink," *International Journal of Engineering Practical Research,* January 2014.

[15] A. C. Pastor, "Conception et réalisation de modules photovoltaïques électroniques," INSA de Toulouse, 2006.

[16] M. R. Patel, *Wind and solar power system*. CRC press, 1999.

[17] R. Boukenoui, M. Ghanes, J.-P. Barbot, R. Bradai, A. Mellit, and H. Salhi, "Experimental assessment of Maximum Power Point Tracking methods for photovoltaic systems," *Energy,* vol. 132, pp. 324-340, 2017.

[18] B. N. Alajmi, K. H. Ahmed, S. J. Finney, and B. W. Williams, "Fuzzy-logic-control approach of a modified hill-climbing method for maximum power point in microgrid standalone photovoltaic system," *IEEE transactions on power electronics,* vol. 26, no. 4, pp. 1022-1030, 2010.

[19] A. A. Ghassami, S. M. Sadeghzadeh, and A. Soleimani, "A high performance maximum power point tracker for PV systems," *International Journal of Electrical Power & Energy Systems,* vol. 53, pp. 237-243, 2013.

[20] G. Abdelmounaim, "An Advanced Neural Network-Based MPPT Controller for Photovoltaic Systems," University of El-Oued, 2023.

[21] https://www.toolify.ai/ai-news/complete-tutorial-implementing-ann-in-matlabsimulink-1764419#google_vignette. (accessed.

[22] https://www.mathworks.com/help/deeplearning/ug/workflow-for-neural-network-design.html. (accessed.

[23] Farh HM, Eltamaly AM, Othman MF (2018) Hybrid PSO-FLC for dynamic global peak extraction of the partially shaded photovoltaic system. PloS one 13(11):e0206171.

[24] Azzouzi M (2012) Comparaison between MPPT P&O and MPPT fuzzy controls in optimizing the photovoltaic generator. Int J Adv Comput Sci Appl 3(12):57–62.

[25] Chekired F, Mellit A, Kalogirou S, Larbes C (2014) Intelligent maximum power point trackers for photovoltaic applications using FPGA chip: a comparative study. Sol Energy 101:83–99.

[26] Rezk H, Eltamaly AM (2015) A comprehensive comparison of different MPPT techniques for photovoltaic systems. Solar energy 112:1–11.

[27] Nabipour M, Razaz M, Seifossadat SG, Mortazavi S (2017) A new MPPT scheme based on a novel fuzzy approach. Renew Sustain Energy Rev 74:1147–1169.

[28] Boukenoui R, Salhi H, Bradai R, Mellit A (2016) A new intelligent MPPT method for standalone photovoltaic systems operating under fast transient variations of shading patterns. Sol Energy 124:124–142.